Determination of Remnant Merger Stage of Equal-Mass Disk Galaxies

A Thesis Submitted in Partial Satisfaction
of the Requirements for the Degree of
Bachelor of Science in Physics (Astrophysics)
at the
University of California, Santa Cruz

by

Taylor Davalos
June 2008

Joel Primack	Dave Belanger
Technical Advisor	Supervisor of Senior Theses, 2007-2008
	Chair, Department of Physics

Abstract

There are many examples of merging galaxy found in observational astronomy, yet the timescales on which merging happens do not allow for one to study the evolution of galaxy merging of any one merger. Furthermore, there are no standard techniques for the identification of the stage of a galaxy mergers progress in the merging process. In this paper, simulations of merging galaxies are analyzed for a variety of collisions of two disk galaxies of equal mass, with the goal of finding a way to help distinguish galactic merger stage through the comparison of observable quantities. The morphology measurements Gini, M20, Concentration, Asymmetry, and Separation in conjunction with photometric color data output, namely the colors LIR/g and NUV-r, are used to this end. LIR/g and NUV-r were found to have a tight correlation with the star formation rate of the galaxies which is in turn related to the merger stage. The approach taken for the identification of merger stage is plotting data in a 3-dimensional observable parameter space with the goal of finding parameters and orientations of the plots to best isolate a merger stage within this space. Special attention is given to the remnant stage of the merger, however the techniques used in this paper could be extrapolated to all other stages as well.

Introduction

Galaxies come in a dizzying variety of shapes and sizes from highly ordered beautiful spiral galaxies like our own Milky Way, to large amorphous balls of stars called elliptical galaxies, to galaxies so strange in their shape and distribution of starlight that it's difficult to know how to describe them. This last mentioned category, the more exotic galaxies observed, commonly labeled as “irregulars”, are often the result of two or more galaxies merging together. These galaxy mergers take billions of years to merge into one larger galaxy, and within this time a lot of interesting things are going on that make them worthwhile to study more closely.

In 1926, Edwin Hubble presented a system of galaxy classification, whereby galaxies were classified as either spirals or ellipticals, with sub-classifications to designate the shape more specifically within each category. The Hubble classification system is often referred to as the Hubble tuning fork, because of the shape of the diagram, as shown in Figure 1. The basic elements characteristic to galaxies of all types, are the disk and spheroid. Spiral galaxies are classified as any galaxy that has a disk as part of its structure, although most spirals, like the Milky Way, have both a disk and a spheroid core of stars. Elliptical galaxies, however, are galaxies without any disk structure at all, and are themselves spheroids. Because mergers have two or more points of high stellar density (one for each formerly independent galaxy), mergers may have multiple spheroids, long, tidal tails, and multiple distorted disks. Mergers most often cannot be classified into the Hubble convention and indeed some of the most exotic and beautiful looking galaxies are in fact merging galaxies. Once a merger is completed, it will tend to form into the amorphous shape of an elliptical galaxy, due to the tidal forces associated with two highly massive gravitational centers, which tend to pull apart whatever disks or spiral arms that may have been present in the galaxies prior to merging.

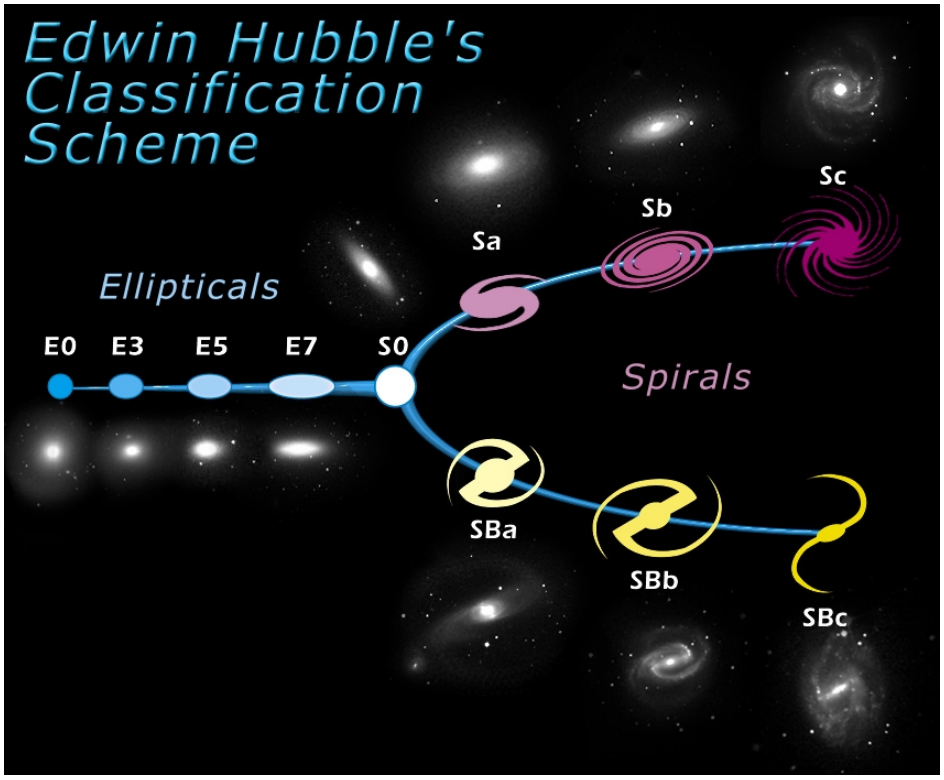

Figure 1. The system of classification of galaxies as either spiral or elliptical, with further sub-classification of the shape of the spiral or elliptical galaxies. The spiral galaxies are divided into two categories, those with or without a barred structure. The barred galaxies are on the bottom.

Galaxies can be the home to anywhere between a thousand and a trillion stars, ranging from dim red K and M stars that can live for hundreds of billions of years to bright blue O and B stars that live only a few million years. Such enormous stars as the O stars burn through their fuel and subsequently explode as supernovae and turn into either neutron stars or black holes, all in a mere blink of the eye compared to galactic evolution timescales. Even with all the stars in galaxies that are merging, however, it is still unlikely for the stars themselves to collide with each other, because the distance between these stars is so vast. Large clouds of gas and dust in each of the merging galaxies, on the other hand, do collide and interact during galaxy merging, and it is in these clouds that new stars are born.

Star formation that was once slow inside each of the individual galaxies increases dramatically during the peaks of galactic interaction. In this stellar breeding ground, one may expect stars of all types being formed. However, because of the relatively short lifetimes of the bigger, brighter, bluer O

and B type stars, one is likely to see a relatively greater abundance of these than in more dormant regions of non-interacting galaxies. Where you see an abundance of these stars you will also find active star formation, since these types of stars will have already burnt out and exploded in regions where star formation is no longer occurring.

Although these brightest stars radiate the most energy toward the blue end of the visible spectrum (compared to our sun, a G star, whose blackbody spectrum peaks in the yellow wavelength region), much of the blue and ultra-violet light that is characteristic to these stars is absorbed by the dust in the same gas clouds in which they were formed. Additionally, radiation that is released when these hot stars explode is also absorbed by this dust which is in turn re-radiated away at longer wavelengths, especially in the infra-red range. Because galaxy mergers exhibit distinct behavior in different ranges of the electromagnetic spectrum, such as infra-red, visible, and ultra-violet light, it would be very useful to be able to make observations in multiple frequency ranges, to get as wide an array of information as possible.

Color photometry is an extremely useful tool for astronomy, because one can take long exposures over a large field of view in a particular frequency band, and get data for hundreds if not thousands of objects at once. Although spectroscopy yields a full spectrum of color and is crucial for examining absorption lines, it is limited by the fact that one may only look at a single object, or a pre-specified and limited number of objects at once, within a greater field of view. Photometry also lends itself well to quantitative measurements of the brightness of astronomical objects because one may compare intensities in various frequency bands to get numerical values of not only the observed luminosity of that object (galaxies in our case), but the relative intensity of two bands. This sort of comparison of an object to itself is more helpful in looking at objects of a wide variety of luminosities. There are many different standardized color bands to choose from and some of these bands will display much more interesting characteristics than others. In this paper we will look primarily at the luminosity in the infrared (LIR), the SDSS g band, SDSS r band, and GALEX NUV band.

Telescopes give us snapshots of only a moment in each galaxies life so it is not feasible to observe a merger throughout the merging process. This is one very good reason why simulations of mergers are so helpful, so that one may study every stage of the merging process. Since one may only effectively get an instantaneous snapshot of a merging galaxy, it is not always obvious which stage of merging the merger is in. Visually, which is to say by examining the observed shape of the galaxy alone, this distinction could be very difficult to make, which is why more quantitative and reliable

methods are needed. This is what will be presented in this paper, with emphasis on the identification of the remnant merger stage.

The simulations in this paper do not take into account the effects of the supermassive black holes at the centers of these galaxies and likewise do not take into account active galactic nuclei (AGN) that are powered by these black holes. There is in fact uncertainty in how the black holes in elliptical galaxies are fed and made to grow more massive. It is a well established observational result that the black hole mass makes up about one thousandth of the mass of the stellar spheroid in which they reside. This means that spiral galaxies, which have relatively small spheroids, will not have black hole of such large mass. When comparable-mass galaxies merge, however, they turn into a single elliptical galaxy, which is spheroid only. The black hole in such an elliptical galaxy will thus be much larger than either of the two constituent black holes, because all of the mass of the spiral galaxies, including the relatively more massive disks, are now part of a spheroid and so with a dramatic increase in total spheroid mass, the black hole mass increases with it. The answer to how the black hole grows so much and why it stops when it reaches this 1/1000 mark is not at all obvious. One theory put fourth in Hopkins et al.. (2007) suggests the black hole terminates its own growth as well as the growth of the spheroid that houses it at the end of the starburst phase of galactic merging. A second and contrary theory forwarded by Ciotti and Ostriker (2007) suggests that the black hole grows independent of merging, controlled by the spheroid itself. It is unclear then, what effect merging itself has on black hole growth.

AGN are observed as high energy radiation emitted from the core of a galaxy, which is due to accretion of surrounding material into the galactic nucleus. The accretion heats the material (gas and dust) as it is pulled in so tightly by the very strong gravitation of the supermassive black hole, giving rise to the high-energy radiation. Where one finds AGN, one will find a growing black hole, and these AGN can be found using high-energy observational bands, although sometimes there is so much gas around the black hole that even energetic X-rays are mostly absorbed. It is not clear, however, whether these bright AGN reside in late-stage merging galaxies, or in elliptical galaxies during roughly a billion years after the merger, because there is no established reliable method of distinguishing between the two. If such a method could be devised, it would then be possible to test which of the theories about the mass relationship between the mass of the spheroid and the black hole is more accurate by examining whether or not merging galaxies are responsible for AGN and hence black hole growth. This is why the distinction of the remnant stage out of all the merger stages, is given special attention in this paper.

Method

There are many different possible mergers to consider, and even viewing very similar mergers can take a drastically different character, depending on the angle from which one observes. The simulations described in this paper all follow a general form, although the mass and types of initial orbit conditions, for instance, may vary considerably. The simulations are initially produced by a program using an N-body/hydrodyanamics program called GADGET written by V. Springel and run by T.J. Cox, that calculates and outputs the motion and behavior of the galaxies as they undergo the various parts of the merging process using an N-Body approach to hydrodynamic calculations, as explained in Cox et al. (2004). A second program called Sunrise, written by Patrik Jonsson, uses monte carlo techniques to model the light from the stars and simulate the effects that dust have on the light as it travels out from the galaxies, as explained in Jonsson (2004). To be as comprehensive as possible, these simulations take into account all the known details about galaxies and their interactions, including the presence and dominance of dark matter toward the total mass, stellar evolution and lifetimes for various types of stars in the galaxies, and the presence and behavior of gas and dust in the galaxies, which in turn drives the star formation. In addition, these simulations have been run with a variety of different supernova feedback parameters in Cox et al. (2006). All simulations are run with the feedback parameter n = 2, meaning that the temperature is proportional to the density ^ 2. The other feedback model with n = 0, is used only for the Prograde-Prograde and Radial (SbcPPn=0 and SbcRn=0) orbit merger simulations (described below), where there is no relation between temperature and density.

All merger simulations begin with two distinctly separated galaxies, which undergo an initial pass through each other, before coming back together and merging at last into the final remnant form. This process is captured from eleven different camera angles for each of the simulations. The reason 11 different cameras are used for any given simulation is that the properties exhibited by a galaxy merger may be obscured in certain directions and not in others. For simulations, where everything can be controlled, one may be temped to look from a perspective that gives the best possible vantage of everything that is happening during the galaxies' interaction, but observationally one cannot expect to be so fortunate. From our telescopes, whether ground-based or in orbit, one only gets a single perspective of any given astronomical object outside our own solar system which is in general a completely random one. Thus, it is important to simulate the same merger from a wide variety of

angles, to be able to anticipate anything an observer may in fact observe. Figure 2 shows the initial pass stage SbcPP merger from camera 0 and camera 5, which give a view of this simulation from above, where one can see the full spiral structure of the galaxies, and from the side, where the same galaxies appear as thin disks. The effect of multiple camera angles on the results of the simulations is that for any given snapshot, and for any given observable quantity, there is a spread of values. One will see general trends arising from the data, but instead of a single definitive value for any parameter at any time, eleven different values will be present, presumably spread around some mean value. In the plots in this paper, all camera angles for all times are displayed on single graphs, to show the greatest possible variety in what one might expect to find observationally.

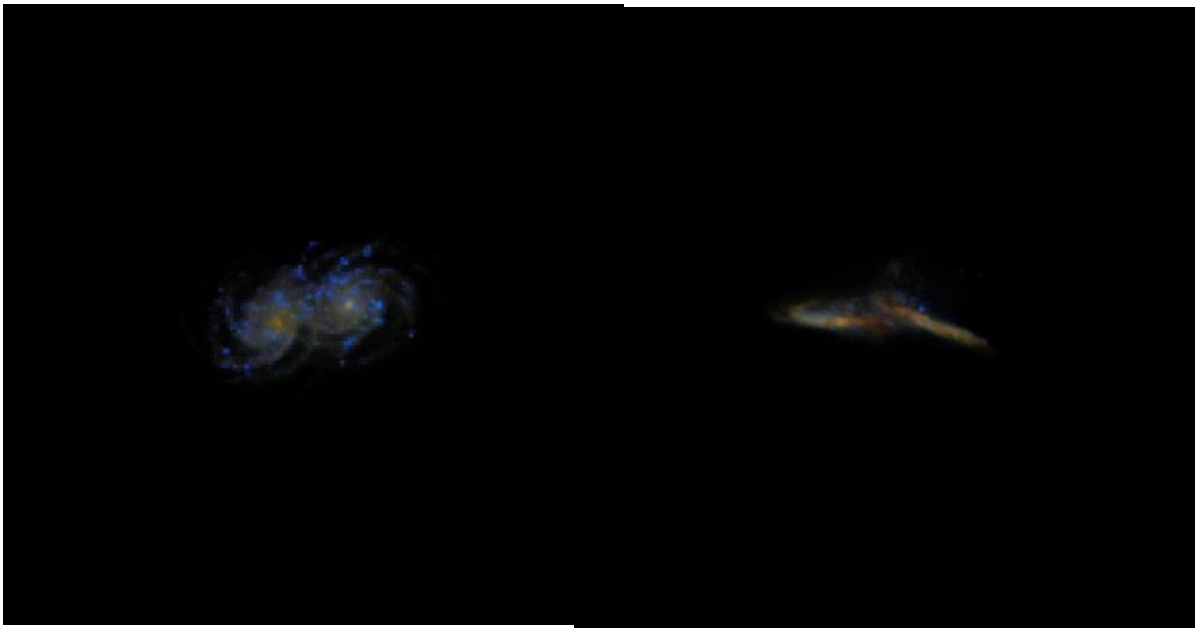

Figure 2. The initial pass stage SbcPP simulation, showing the same galaxies coming together for the first time in the initial pass as viewed from above (Camera 0) and from the side (Camera 5). These two cameras show the two extremes in vantage point, which is to say Camera 0 gives the most directly "overhead" view and camera 5 gives the most sidewards view of the galaxies.

There are two basic categories of merging galaxies analyzed in this paper; a series of Sbc galaxies of varying types of initial orbits, and a set of G galaxies of varying sizes. The Sbc simulations are so named because the galaxies, prior to merging, are classified as Sbc in the Hubble classification system (see Fig. 1). The Sbc (with lowercase "b") means that these galaxies are unbarred spiral galaxies with a type of spiral structure in between what would be classified as Sb or Sc. The Sbc simulations are also given a designation to indicate the kind of initial orbital conditions of the galaxies.

The SbcPP, SbcPR, and SbcRR galaxies are nearly parallel to one another at the beginning of the simulations, having their axes of rotation tilted toward each other at an angle of about 30 degrees. These three mergers, along with the SbcPl simulation, all have a pericentric distance, the distance of closest approach, of R_{peri} = 11 kpc for their first pass. The SbcPP galaxies (both type Sbc) each have a prograde rotation, relative to their direction of orbit. In other words, the galaxies are rotating in the same angular direction as the rotational direction of their initial approach toward each other. For the SbcPR simulation, one galaxy has a prograde rotation, as just described, while the other has a retrograde rotation. Retrograde is the opposite kind of rotation as prograde; the galaxy is rotating in the opposite way of the incident rotation of the galaxies orbiting each other. The SbcRR galaxies are both rotating in a retrograde motion relative to the direction of their orbits to each other. The galaxies in the SbcPl simulation have a polar orbit, meaning that their axes of rotation are at about right angles to each other, as they orbit toward each other.

Figure 3 shows the pre-merger stage of the SbcRR and SbcPl simulations. The SbcPl galaxies are oriented so that their axes of rotation are at right angles to one another. The SbcRR appears similar to how all of the Sbc mergers besides the SbcPl would look at this stage in a still frame. In order to get a good appreciation of how these simulations differ, one should take a look at the animations of the mergers, which are available free for download at http://governator.ucsc.edu/simulations.

Figure 3. The pre-merger stage of the SbcRR simulation (left) and SbcPl simulation (right), as viewed from the same perspective. The SbcRR galaxies have nearly parallel orientations, while the SbcPl galaxies are tilted at right angles to each other.

Three other orbital types were examined for this paper in the SbcPPr-, SbcPPr+, and SbcR simulations. The SbcPPr- and SbcPPr+ simulations both have prograde motion for both of the incoming galaxies, but with different pericentric distances, compared to the SbcPP simulation. The SbcPPr- has the shorter distance of closest approach on first pass of R_{peri} = 5.5 kpc, while the SbcPPr+ has the larger value of R_{peri} = 44 kpc. The galaxies in the SbcR merger have a prograde-retrograde orientation, similar to the SbcPR merger described above, although the orbit itself is highly radial, meaning that the galaxies do not swing around each other as they do in the other simulations, but rather fall almost directly into each other, for a much more head-on collision than any of the other mergers.

The other class of galaxy mergers analyzed, the G-G galaxies, have less gas and dust than the Sbc series. All of the G-G mergers have a prograde-prograde orientation, like the SbcPP simulation described already. While the two constituent galaxies of each of these mergers have the same mass, simulations for a number of different masses have been run and the G-G galaxy mergers are numbered to indicate their relative mass stating with the lightest G0G0 merger. Each galaxy of the largest merger, the G3G3 merger, has a total mass of 1.2 trillion solar masses, whereas the Sbc galaxies have a total mass of 0.81 trillion solar masses. The galaxies of the smallest merger, the G0G0, have a mass of 51 billion solar masses, a factor of 23 less than the largest. This mass, includes both the baryonic matter as well as the dark matter halo, which comprises about 90% of the total galactic mass, on average. For more details about the initial galaxy properties, please refer to Table 1 of Lotz et al. (2007).

The full timescale for mergers depends on several factors including size of constituent galaxies and the type of orbit they have with one another, however several salient characteristics hold for all simulations and from these a convention of merger stage may be constructed. The entire history of a galaxy merger, which lasts typically between 2 and 4 Gyrs, is broken down into six separate stages; pre-merger, first pass, maximal separation, final merger, post merger, and remnant. These stages are based on the time at which the galactic centers are at a minimal distance during the first pass (t_{fp}), and later at a maximal distance during the maximal separation stage(t_{max}), before the coalescence of their galactic nuclei during the final merger stage (t_{merg}). These stages are defined as follows. The pre-merger spans from the beginning of the simulation until 0.5 t_{fp}. First pass goes from 0.5 t_{fp} to 0.5 (t_{fp} + t_{max}). The maximal separation stage extends from 0.5 (t_{fp} + t_{max}) until 0.5 (t_{max} + t_{merg}). The final merger stage encompasses the final coalescence of the galactic nuclei and is defined from 0.5 (t_{max} + t_{merg}) until t_{merg} + 0.5 Gyr. The post merger stage lasts from t_{merg} + 0.5 Gyr until t_{merg} + 1.0 Gyr. Lastly, the remnant stage extends from t_{merg} + 1.0 Gyr until the end of the simulation.

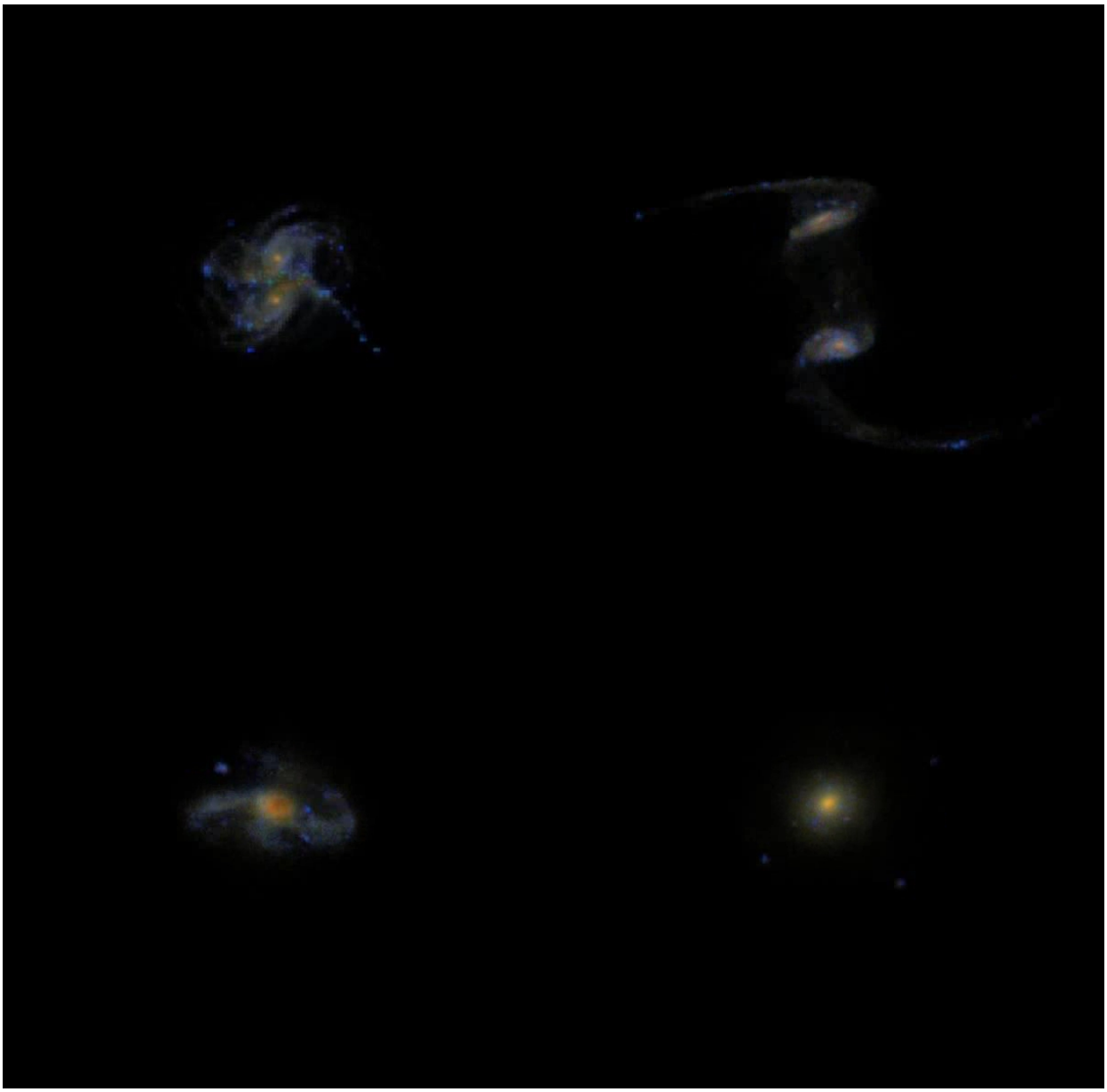

Figure 4. Various merger stages. Clockwise from the upper left: SbcPPr- initial pass, SbcPP maximal separation, SbcPP remnant, and SbcPP final pass.

For the purpose of familiarizing the reader with the various stages of merging, Figure 4 shows the initial pass, maximal separation, final pass, and remnant phases. For comparison, Figure 5 shows some merging galaxies captured by the Hubble Space Telescope which were recently released. More of these images may be found at http://hubblesite.org/newscenter/archive/releases/2008/16/.

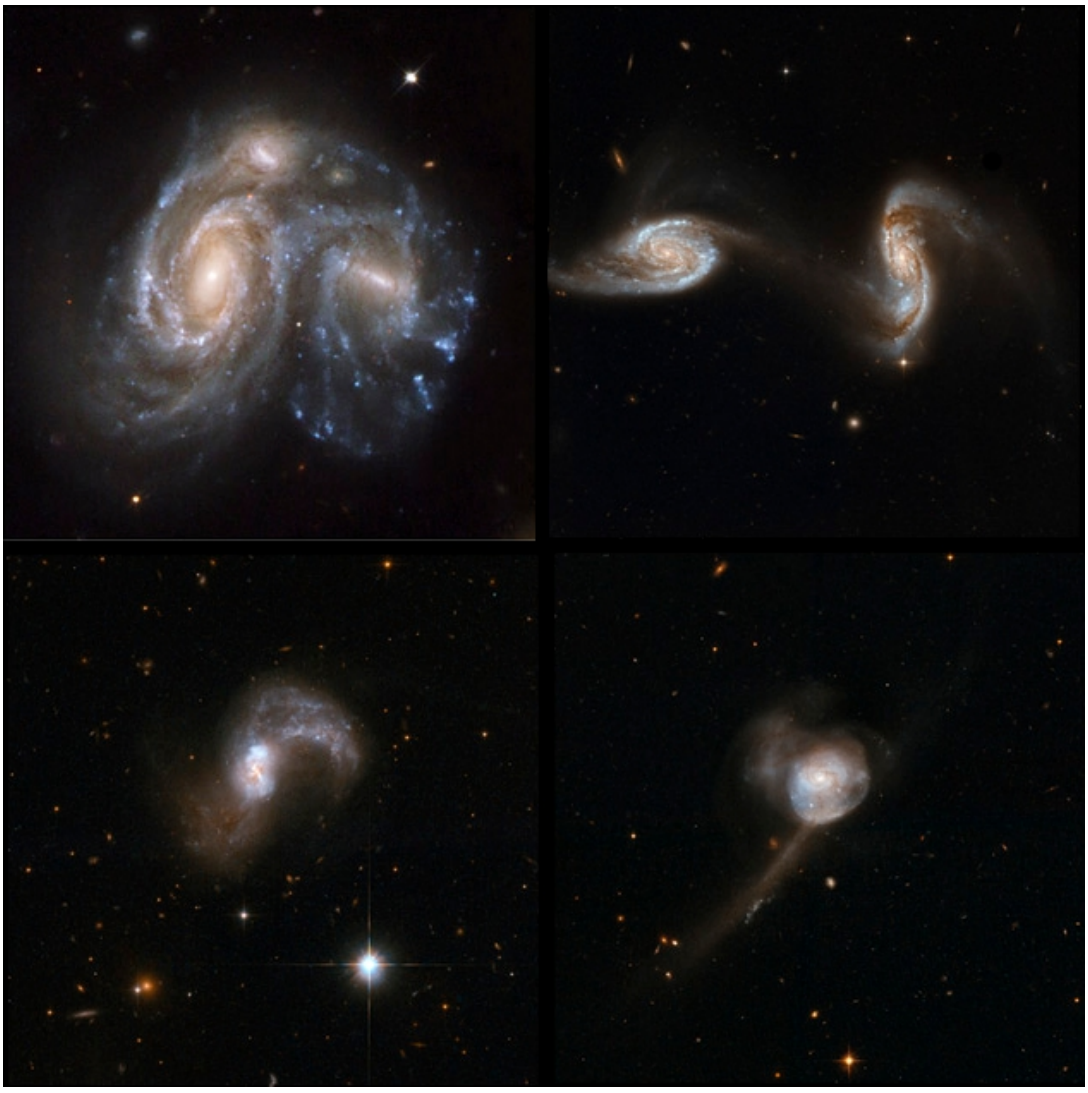

Figure 5. Hubble images of merging galaxies in various merging stages.

To distinguish between various types of galaxy interaction, especially at higher redshift, where a high resolution image may not be available, it is useful to examine the distribution of light intensity in an image in a quantitative way, to get a systematic measure of the "shape" of the galaxy, called morphology, and there are several pre-established quantities that shall be used in this paper, some of them more recently developed than others.

Before one can make any quantitative measurements of a galaxy, one needs to be able to distinguish what parts of an image may actually be considered considered part of a galaxy, and which parts are to be ignored. This is done with segmentation mapping by a program called Source Extractor, which classifies regions of the image as being either part of a galaxy or not, based on whether the

image crosses a certain brightness threshold. The segmentation map looks for two separate objects and labels them A and B. If the galaxies are too close together for the segmentation map to be able to distinguish between them, it classifies both objects as one object and labels it as the “A” galaxy. In this case, the morphology information that would normally go into the “B” galaxy is assigned the preposterous value of -99 and is given a tag to notify that this data is not to be used. In the plots that follow, information from the primary “A” galaxy is plotted with “+” symbols, while the data from the secondary “B” galaxy, when used, is plotted with “x” symbols. It is now possible to define morphological data in a firm, quantitative manner.

Separation is the easiest of all the morphological measurements to “see” because it is a simple determination of the distance between the two galaxies' centers, as determined by the segmentation map, measured in kiloparsecs (one kiloparsec is equal to 3259 light years or about 3.08*10^16 kilometers). If the segmentation map is unable to distinguish between the two galaxies, separation is given a value of zero. Separation depends highly on viewing angle because if one galaxy is obscuring the view to the other, the segmentation map will not be able to see them as two separate objects and separation will have the false value of zero, while they may be a substantial distance apart. Separation is a very useful tool for dividing the data into two separate domains, based on whether or not a distinction can be made between the galaxies. Separation is used in this paper to reduce the amount of data in a simulation to a more manageable amount, by separating the data into zero or non-zero sets. Separation should not be used as a sole criterion for merger stage determination because of the likelihood of “false zeros” as already described. Figure 6 shows a plot of the separation of the galaxies, as a function of time, for all camera angles.

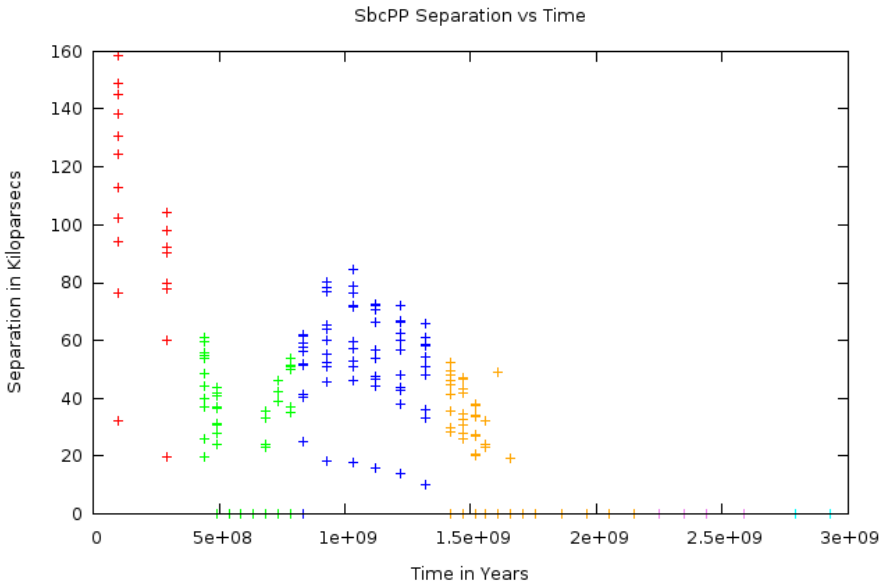

Figure 6. A plot of Separation vs Time for the SbcPP simulation. Some values of zero are due to the galaxies going through one another or merging as one, while others are caused by one galaxy obscuring the other from a particular camera's perspective.

Gini is a quantity borrowed from economics that is a measure of the nonuniformity in the distribution of wealth in a population (Glasser 1962). In the context of astronomy, gini is a measure of how unevenly distributed the light is in a given image of a galaxy (Abraham et al.. 2003, Lotz et al.. 2004). Gini is measured by normalizing the brightness of the pixels (total flux made to equal unity) and arranging all the pixels in a snapshot in order of dimmest to brightest. The next step is to define a function S(k) that is a sum of the first k pixels in the ordered list, where N is the total number of pixels in the image. If we call F_1 the dimmest pixel, F_2 the second dimmest, up to the brightest pixel F_N, then

$$S(k)=F_1 + F_2 + ... + F_k \quad \text{for } (0 \leq k \leq N) .$$

If the pixels have a uniform distribution of light, S(k) will look like the straight line S(k)=k from k=0 to N. If, however, the pixels to not have a uniform distribution, that line will have the same boundary values but it will sag down toward its beginning, due to the less illuminated pixels being the first ones in the ordered list. The more unevenly distributed the light is in the image, the greater this effect will be.

Gini is defined as

$$G = 1 - 2[\sum S(k)]/N.$$

That is, gini is the difference between a perfectly even distribution of light (the straight S(k) line mentioned above), and the actual light distribution curve, numerically integrated over all values of k. The maximum value of G=1 corresponds to a case where all the light is focused into a single pixel while the minimum value of G=0 would correspond to the case where the light is perfectly evenly distributed between all pixels. Graphically it is the area between these two curves, as seen in Figure 7.

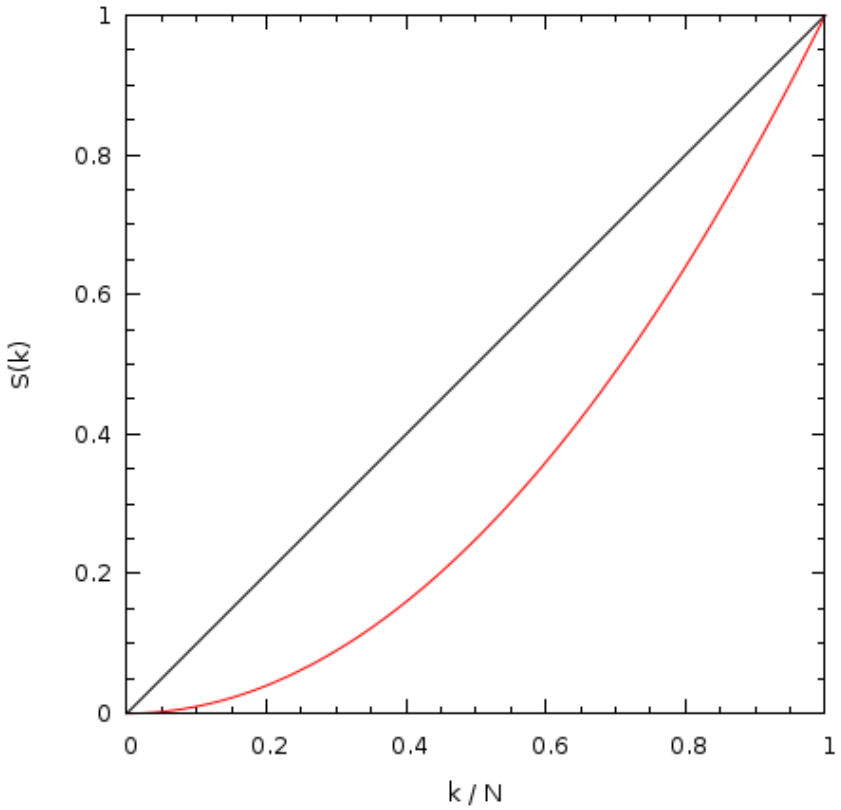

Figure 7. Grapical representation of gini. Gini is defined as twice the area between the two lines. The more unevenly distributed the light is within the segmentation map, the greater gini will be.

M20 is a quantity that describes how concentrated the light is relative to the galactic center (Lotz et al. 2004). Let M_i equal $(f_i)(R_i)^2$, the brightness of the i^{th} pixel times the square of the distance from that pixel to the galactic center. M_{tot} is the summation of M_i over all pixels. The center of the image is defined to be the point which minimizes M_{tot}. We may now define M20 as

$$M20 = \log_{10} ((\Sigma_i M_i) / M_{tot}),$$

where the summation of M_i is taken over the brightest 20% of the pixels. Because $\Sigma_i M_i$ is always going to be smaller than M_{tot}, M20 will always be negative. The quantity M20, then, is a measure of how concentrated the light of a galaxy is about the galaxy's center; the lesser the value, the more concentrated the light is toward the center of the galaxy, and vice versa. In the graphs containing the value of M20, the M20 axis is negatively oriented so that lower values of M20 are further from the graphical origin.

Concentration is is defined as the log of the ratio of the radius containing 80% of the galaxy's total flux to the radius containing 20% of the galaxy's total flux, multiplied by 5.

$$C = 5 \log_{10}(r_{80} / r_{20})$$

The more focused the light is toward the center of the galaxy, the larger concentration will be. Concentration was invented and put into use well before M20 was, although the two quantities measure very closely related things. Concentration, however, has the drawback that it makes the assumption that the brightest 20% of the pixels are in fact the ones closest to the center. For a more irregular distribution of light, as is often the case in mergers, this may not necessarily be the case, which is why M20 is such a useful quantity, since it does not make this assumption.

Asymmetry is a measure of how rotationally asymmetric a galaxy is. This is done by rotating the image of a galaxy by 180 degrees about the center, and subtracting this image from the original. The center is defined to be that point which minimizes Asymmetry.

$$A = (\Sigma_{i,j} | I(i,j) - I_{180}(i,j) |) / (\Sigma_{i,j} | I(i,j) |) - B_{180}$$

where I is the image of the galaxy, I_{180} is the rotated image, and B_{180} is the average asymmetry of the background. Asymmetry will be very low for galaxies like ellipticals, and will be very high for asymmetric systems like a merging galaxy, making it a good indicator for distinguishing galaxy merger stages. Asymmetry does not work so well for low signal to noise ratios, however, because in subtracting the rotated image from itself, you lose information that may have been either signal or noise. If the noise is high, compared to the signal, what you subtract may not be the galaxy itself, but randomness that will affect the accuracy of asymmetry.

Galaxies emit not only visible light, but light of wavelengths that span the entire

electromagnetic spectrum. The intensity of light that is released in a given band of frequencies depends on a number of factors, including the star formation rate, the presence of dust, and the size and luminosity of the galaxy as a whole, just to name a few. To give the brightness of a galaxy within a single frequency band is not particularly useful because such a quantity would have no meaning without how bright that is in context of any other measurements. For example, a high value of light emitted in an infra-red band could signify a normal sized galaxy undergoing a period of high star formation rate, or it could just be the result of a particularly large galaxy, emitting that much more light in all frequency bands. For this reason, it is more helpful to compare the relative brightness in two different frequency bands for the same image. This way, one can see how relative intensities in various bands change. Now, by looking at at the luminosity in the infrared compared to luminosity in the green band, for instance, one can tell that one or the other is especially high or low, regardless of the galaxy's size or other factors. Such a process is particularly helpful when examining a wide range of galaxy types and orbits, as is the case for this paper.

In astronomy, a color is defined as being the difference in magnitudes between two different frequency bands. A magnitude is a measurement of brightness, originally defined so that the dimmest stars one can see with the naked eye have a magnitude of 5, while the brightest have a magnitude of zero. More quantitatively speaking, magnitude is a logarithmic scale that increases in observed luminosity by a factor of 100 for a *decrease* in five magnitudes, or a factor of about 2.5 in luminosity for one magnitude. Higher magnitudes mean dimmer objects, while lower magnitudes mean that an object is relatively bright.

There are many different color filters commonly used throughout the astronomy community. The filters that are used in this paper, a few of those output from the simulations, are SDSS filters and GALEX filters. In particular, the SDSS colors g (for green) and r (for red) as well as GALEX NUV (near ultra-violet) are used extensively. As a reference, all of the SDSS and GALEX filters are shown in the Figure 8, as they are defined for these simulations. LIR (Luminosity in the Infra-Red) is the other measure of light intensity used in this paper. LIR is defined simply as the amount of light absorbed and re-radiated by dust and is between roughly 5 μm and 1 mm in wavelength.

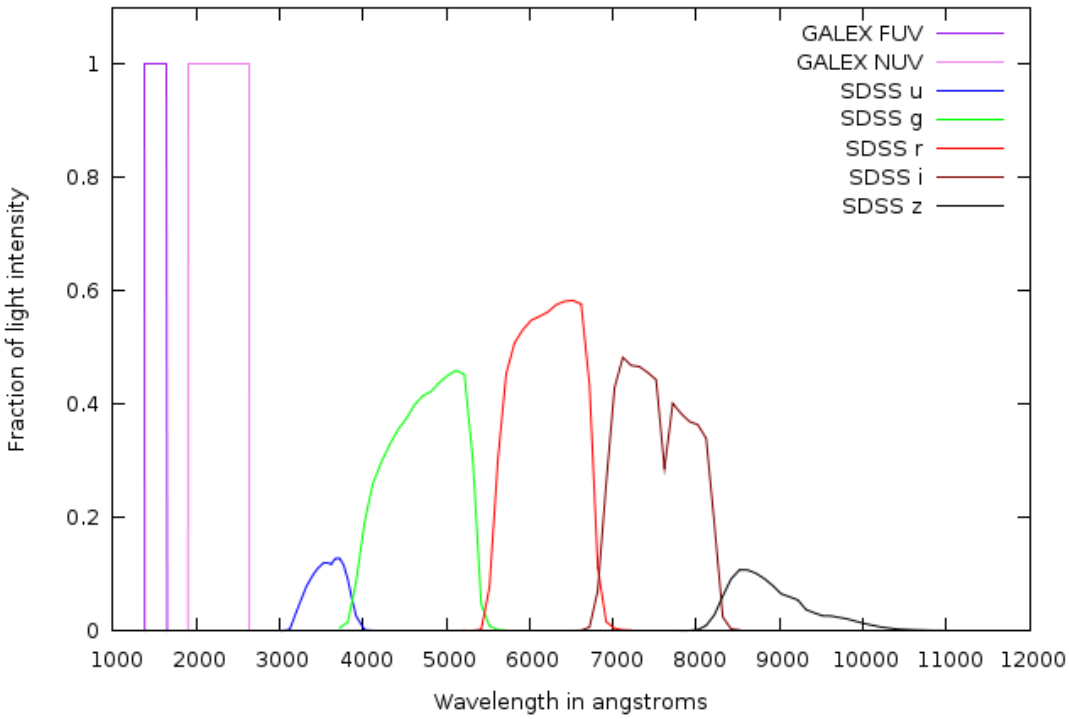

Figure 8. Plot of GALEX and SDSS color filter bands. The bands used in this paper are GALEX NUV, SDSS g, and SDSS r.

The merger stages are made distinct in the various graphs in this paper by designating a color to each one, regardless of specific merger parameters. These colors are chosen to be consistent with the Lotz et al. (2007) and are as follows: pre-merger is red, first pass is green, maximal separation is blue, final merger is orange, post-merger is violet, and remnant is cyan. These merger stage colors are illustrated with the following plot in Figure 9.

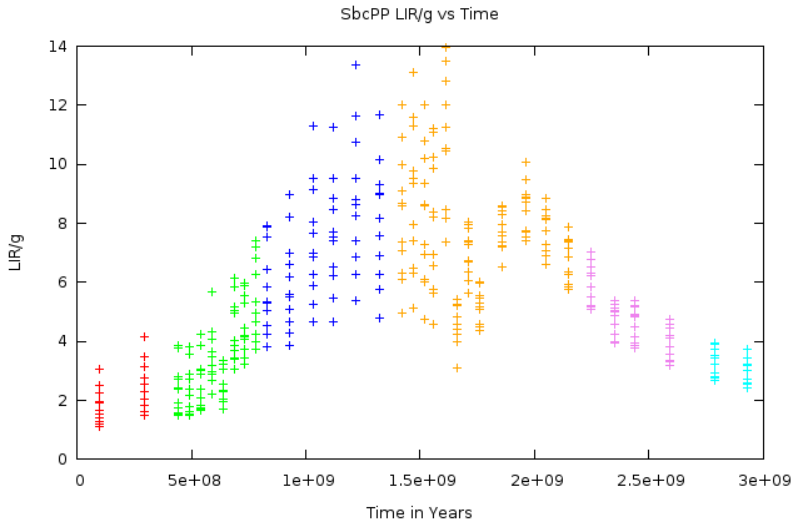

Figure 9. A plot of LIR/g vs Time, intended to show the order of merger stage colors.

The surface plot (splot) function of Gnuplot allows one to make 3 dimensional plots of mathematical surfaces as well as 3 dimensional plots of data. These 3 dimensional plots are fully rotatable in the output display of Gnuplot. Shown below is a plot of "LIR/g vs Gini vs M20" for the G3G3 merger simulation. The upper left image of Figure 10 shows this plot from directly above, thus showing only Gini and M20 values, with LIR/g indistinguishable, due to the angle of orientation. It is only when the plot is rotated, as shown in the subsequent images, that the LIR/g color may be clearly seen. It is possible to find an orientation such that the different merger stages, indicated by color, can be made to appear is distinct as possible. This is done in the subsequent plots in Figure 10, below. Notice, in particular, that the cyan remnant stage is buried in nearby data in the first, unrotated image, however in the final rotated image, it has a clearly distinct region in this 3-d parameter space.

As in Figure 10, if one were to look directly down the z axis (the color axis) of any of the 3-d plots in this paper, one would see the morphology alone, without the added distinction that the color (difference between bands) adds. Such strictly morphological plots may be found in Fig. 19 of Lotz et al. (2008).

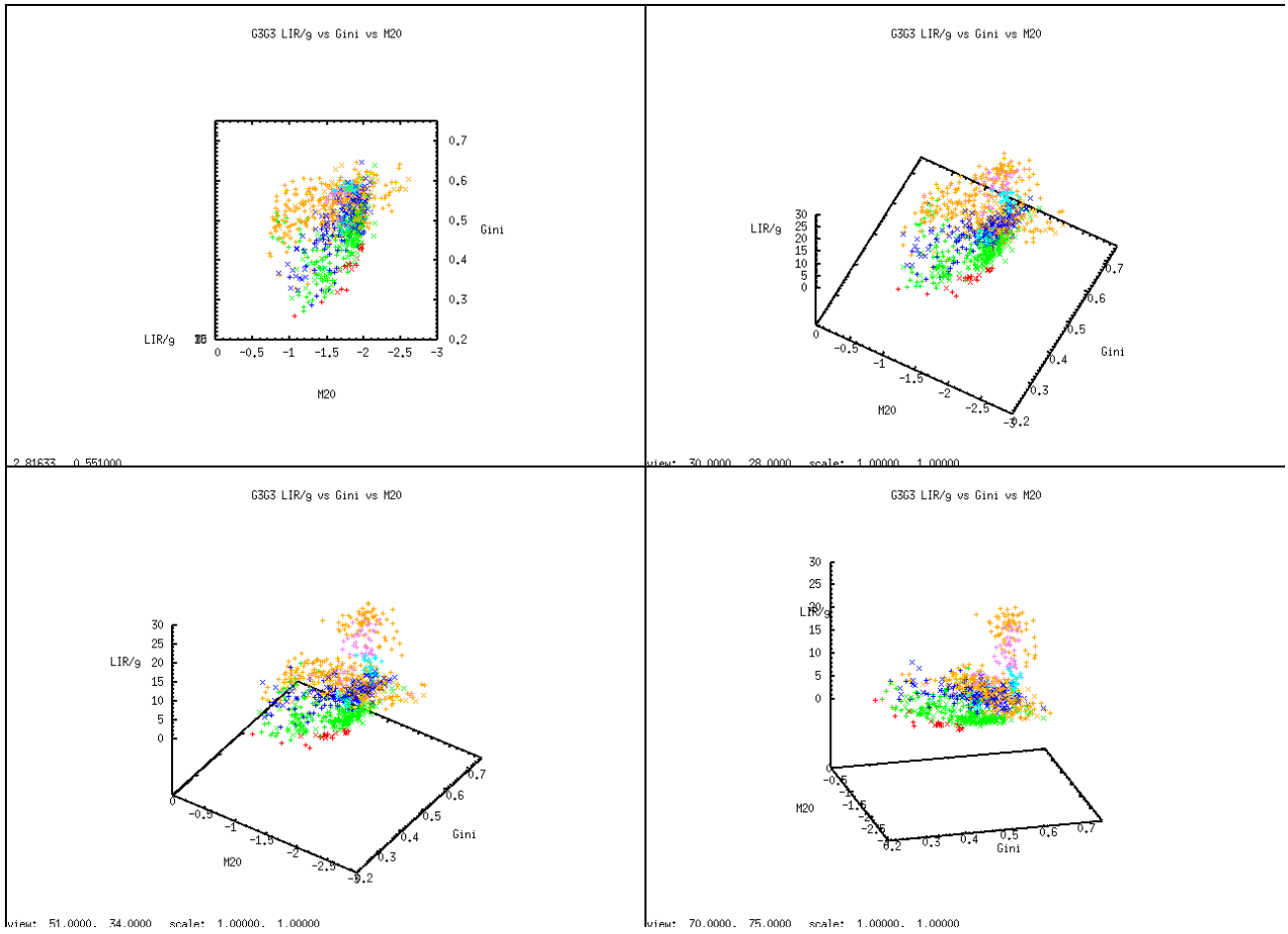

Figure 10. Demonstration of rotation of 3-d graphics with GNUPlot

Results

The presence of dust in the simulations has a significant effects on the numerical values for the intensity of light in the colors examined. For any given snapshot for any given merger, there will always be a spread in the values of any color based on the angle from which the image is taken because there will be more dust obscuring the view of the galaxy in some directions than in others. This is illustrated in Figure 11, which is a plot of the attenuation effect that dust has on NUV-r in the SbcPP merger. The attenuation in this plot is calculated by subtracting the values of NUV-r of the galaxies without dust, from the corresponding values of NUV-r of the same galaxies with dust. Values of this absorption from Camera 0 and Camera 5 have been plotted with special characters (hollow squares and triangles, respectively) to distinguish them from other cameras. Recall from Figure 2 that Camera 0 has a viewpoint directly above the galaxies, with a line of sight parallel to the galaxies' axes of rotation, while Camera 5 gives a viewpoint most directly to the side of the galaxies, giving a view perpendicular to the galaxies' axes of rotation.

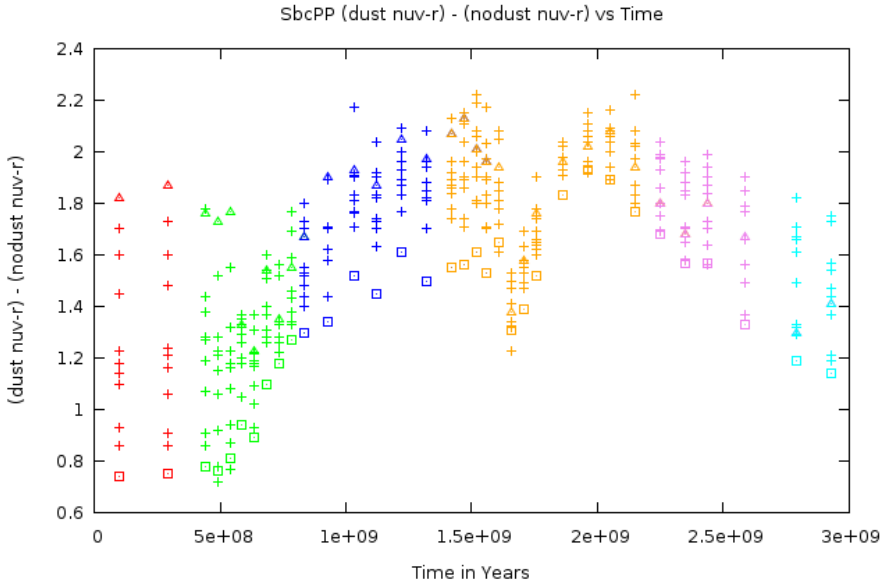

Figure 11. The attenuation of NUV-r from the presence of dust. The greatest variance in attenuation is in the pre-merger stage. The side-view of Camera 5 (triangles) experience the greatest attenuation because the light has to travel through the most dust to reach the camera. The top-view of Camera 0 (squares) has the lowest attenuation for the opposite reason.

This Figure 11 shows that the spread in NUV-r over the 11 camera angles is the greatest in the pre-merger stage, before the galaxies have had any chance to interact. Not only that, but the attenuation of NUV-r by the dust is the lowest for Camera 0 and the greatest for Camera 5 in this pre-merger stage. The reason for this is that the light from the galaxy has to travel through the most dust in order to reach Camera 5, since sideways from the disk is the thickest path of escape for the light and additionally, the disks are the most orderly at the beginning of the simulation, before tidal forces can begin to destroy them. In contrast, the light escaping from the flat surface of the disks has the least amount of dust to pass through in order to reach Camera 0. For all the plots that follow, then, it is helpful to keep in mind this effect, and how drastically perspective can alter the values of colors for the same object at any given time.

The value for LIR/g has a positive correlation with the star formation rate. The greater the star formation rate, the greater is the infra-red luminosity compared to the luminosity in the green portion of the visible spectrum. This is saying more about the infra-red luminosity than the green band, since the green luminosity remains relatively unaffected by the merging process. This is shown by comparing plots of infra-red and green luminosity, as shown in the Figure 12.

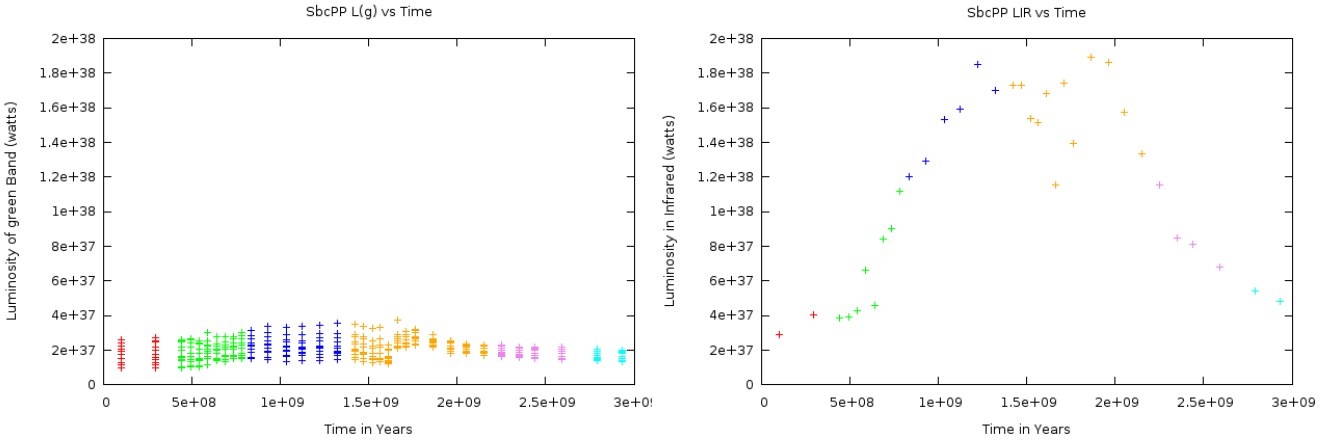

Figure 12. A comparison of green and infra-red luminosities in the fiducial merger. Notice how the green remains relatively constant while the infrared jumps by a factor of ten during the simulation.

One would indeed expect this rise in infrared luminosity to correlate with the rise in star formation rate because, as mentioned in the introduction, the young, bright, massive stars that are prone to explode soon after their birth, heat up the dust in which they were formed, which then emits light in the infrared range.

NUV-r is the other color used extensively in this paper and was shown in the observationally based Salim et al. (2007) paper that this would be a good indicator of star formation. This paper was brought to our attention after the simulations had been run. Once the plots were made from these simulations, we confirmed that NUV-r does indeed correlate with the star formation rate. This goes to show that our models correlate well with observations, since the simulations were not made to mimic such an effect, but rather produced it naturally, without a priori knowledge of it. We now can see that NUV-r can be a very helpful tool for determining galactic merger stage.

NUV-r decreases with increasing star formation and increases again as the star-formation dies off. Bear in mind, however, that magnitudes are an inverse scale, so a relatively low value of NUV-r in fact indicates a relatively high intensity of near ultra violet light. In general, the nuv band is more dynamic than the r band throughout the merging process, as shown in the comparison in Figure 13. There are two key things to notice in this comparison. The first is that there is a greater spread in the values of NUV over the 11 camera angles than the values of r. This indicates that NUV is strongly attenuated by dust, as explained earlier, and that the dust has a stronger effect on ultra-violet light than visible light. The second, and even more significant thing to notice is that the data of the NUV plot follow a steeper slope towards the beginning and end of the merger. Remember that the creation of young, giant, stars produces a lot of bluer (including stronger UV) light than would be present at times of low star formation, since these stars don't live for very long. So now we can see, in particular, that the more pronounced rise in magnitude at the after the coalescence is due to the decaying star formation as the galaxies settle into a less perturbed and less star-forming elliptical galaxy.

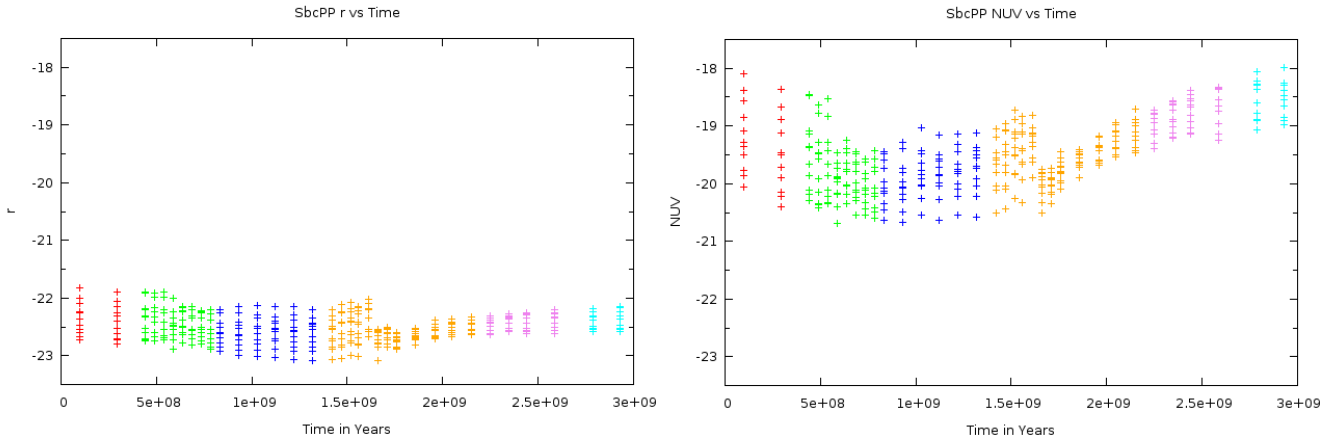

Figure 13. A comparison of the r and NUV bands throughout the merging process. The stronger spread of NUV is due to stronger dust effects. The steeper slope is due to greater sensitivity to star formation.

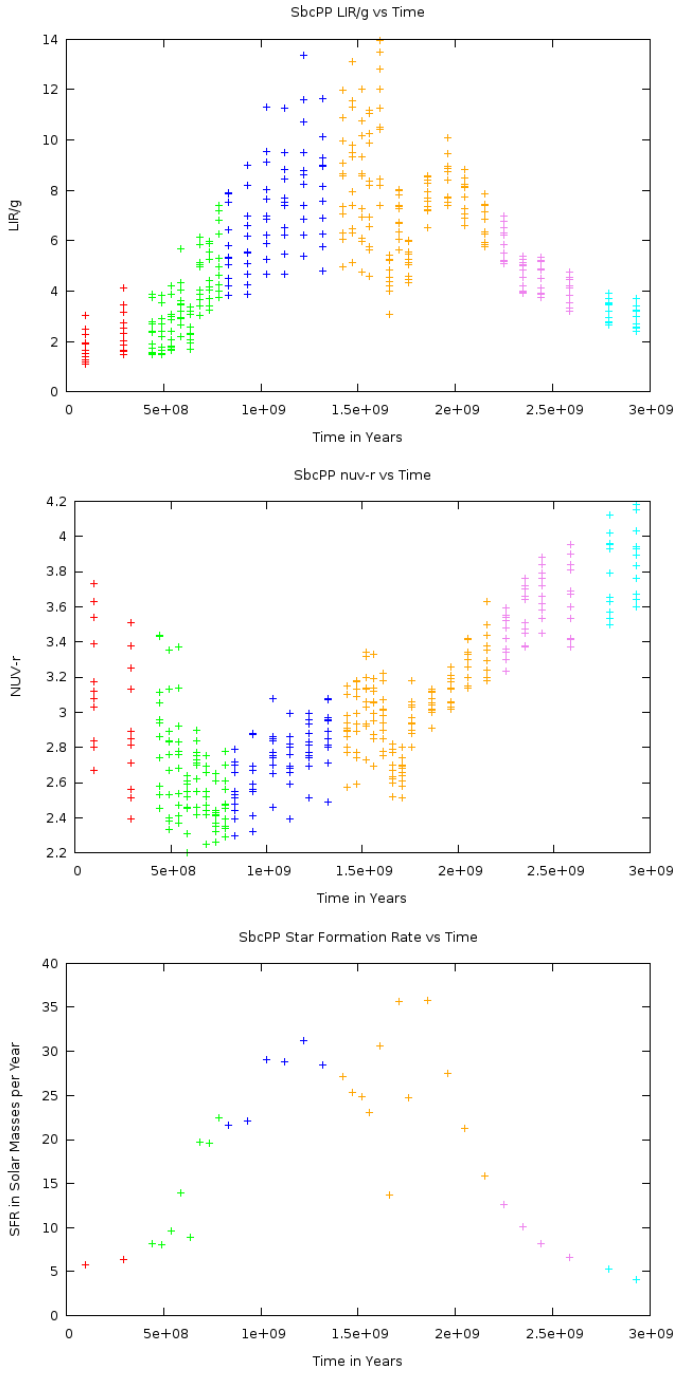

Figure 14. Plots of LIR/g, NUV-r, and star formation rate vs time, for the SbcPP merger, for comparison to one another. As star formation increases, LIR/g increases and NUV-r decreases. When star formation rate decreases, LIR/g also decreases, while NUV-r increases.

With these correlations of NUV-r and LIR/g to star formation in mind (see Figure 14 for a comparison), it is now appropriate to examine some data using these colors in conjunction with morphology data, to get some insight into how to make the distinction between various merger stages, particularly the remnant stage. It is fairly easy to see the general trends of NUV-r and LIR/g as they relate to star formation when plotted linearly with time, as in Figure 14, for the SbcPP simulation. Similar plots for all the other simulations may be found in the Data section of this paper.

Merging is a process that takes billions of years, so it is not possible to see any appreciable change in any quantity over time. What one observes is only instantaneous images of a dynamic process that lasts on the order of a hundred million times longer than the life of any astronomer. What is required, then, is a way of determining merger stage independent of any reference to time. Graphically, we seek a perspective on plots of observable parameters that make the distinction of the color-coded merger stages as clear as possible, and as general as possible for all merger types.

Figure 15 is a plot of Gini vs M20 for the SbcPP merger. Notice how the cyan remnant stage is localized within the range of -1.5 > M20 > -2 and 0.5 < Gini < 0.55. Compared to the rest of the data in this plot, the brightest pixels of the remnant stage light are confined to a relatively small radius (relatively low M20) and the total amount of light is fairly unequally distributed throughout its images (relatively high Gini). This relatively confined region is a good start, but note also how the presence of other stage data, notably the orange final merger stage and the violet post merger stage, clutters up this same region, making it ambiguous whether any random data in this region belongs to any particular stage.

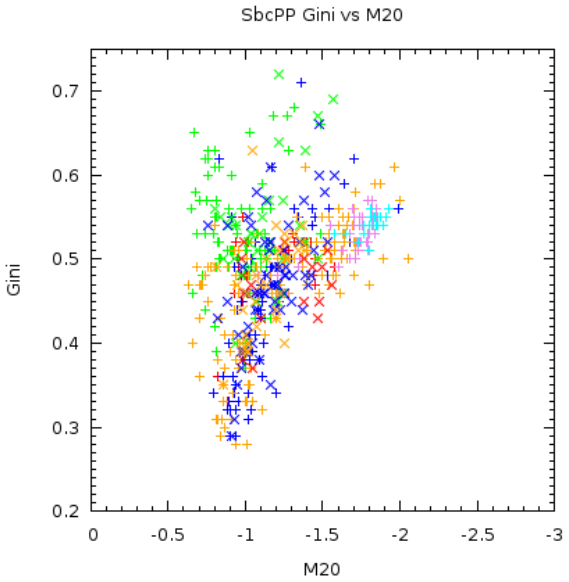

Figure 15. A plot of Gini vs M20 for the SbcPP merger. The cyan remnant stage is fairly localized,

however not completely distinct from the surrounding data.

Figure 16 is a plot of the same gini vs M20 data for the same simulation, now plotted against NUV-r in the z-axis of this 3-dimensional plot. Plotting with a third color axis in this way helps to spread the data over another spatial direction of the graph. Notice how the same cyan remnant stage data is now more distinct from the surrounding violet post merger data, and especially more distinct from the orange final pass stage that cluttered the remnant region in the previous 2-dimensional plot of Gini vs M20 alone. The viewing angle of this image is chosen in such a way to augment this distinction of the remnant region. From such an angle, one can see that the remnant stage resides in the far upper corner of the data.

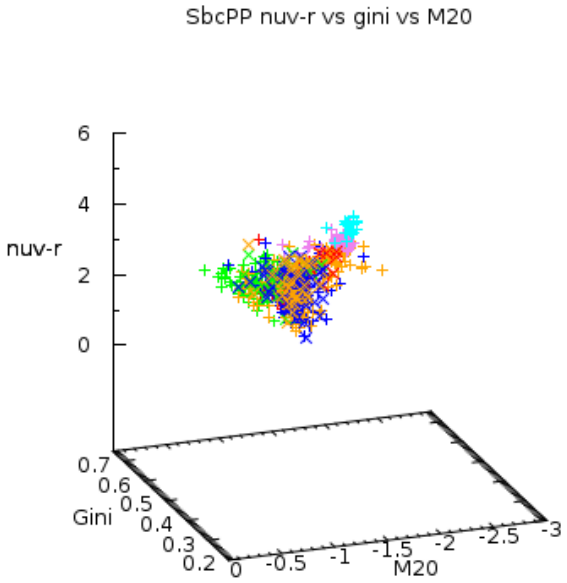

Figure 16. 3-D plot of NUV-r vs Gini vs M20 for the SbcPP simulation. Notice the distinct cyan remnant region in the far upper extreme of this plot view.

This isolation of the remnant stage shown above is a fairly general result across all simulations examined in this paper. The SbcPP merger is used here, as throughout this paper, as a point of reference to all the other simulations, but it should not be mistaken for a case that necessarily illustrates this separation of remnant stage better or worse than any other simulation. The isolation of the remnant phase into the region where it resides above is a general result for all the simulations examined.

Although there is naturally some deviation between them, the result holds fairly well, considering the range of different initial conditions between differing simulations. Figures 17 and 18 are similar plots of Gini vs M20 as well as NUV-r vs Gini vs M20 with the same viewing angle of the 3-d plot, except now the data for the SbcPPr- simulation has been plotted instead of the SbcPP data. Similar plots for the rest of the simulations may be found in the data section.

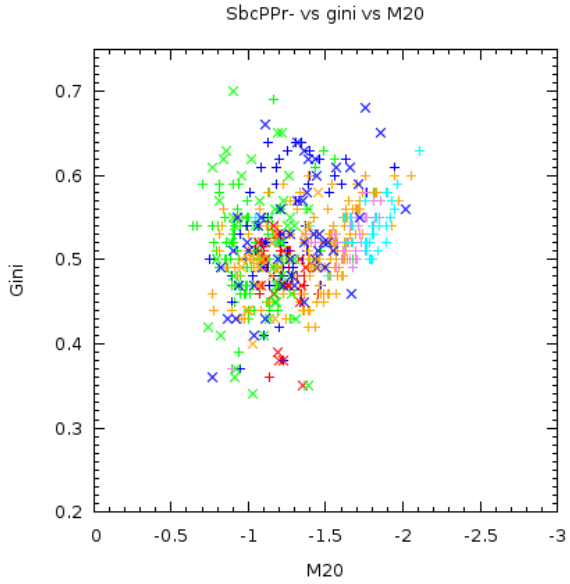

Figure 17. Plot of Gini vs M20 for the SbcPPr- simulation.

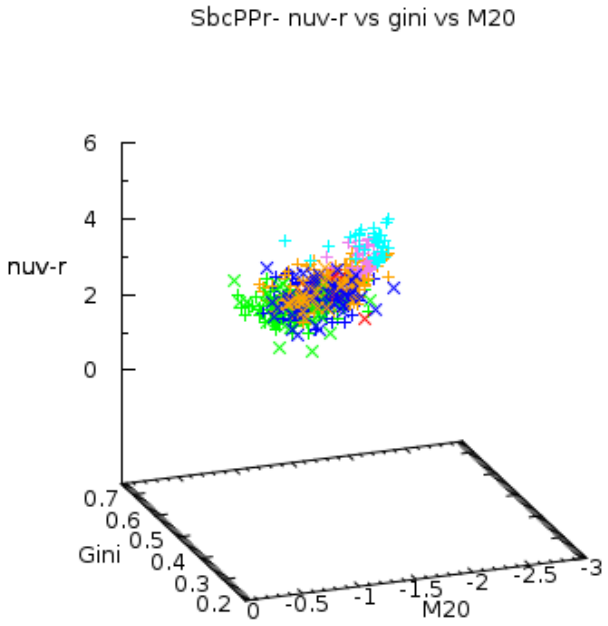

Figure 18. Plot of NUV-r vs Gini vs M20 for the SbcPPr- simulation. Notice, as in the SbcPP plot of

the same parameters, the localization of the cyan remnant stage data into the same general region, namely the far upper corner of the data plotted.

As mentioned in the method section, it is possible to remove a large portion of data from a plot by focusing only on points for which the separation is equal to zero. This was done for plots of LIR/g vs Concentration vs Asymmetry, which made the distinction of the remnant stage in these plots particularly clear. The first of the following three plots (Figure 19) is that of Concentration vs Asymmetry without LIR/g. As with Gini vs M20, the cyan remnant stage is localized within a characteristic region for nearly all the simulations.

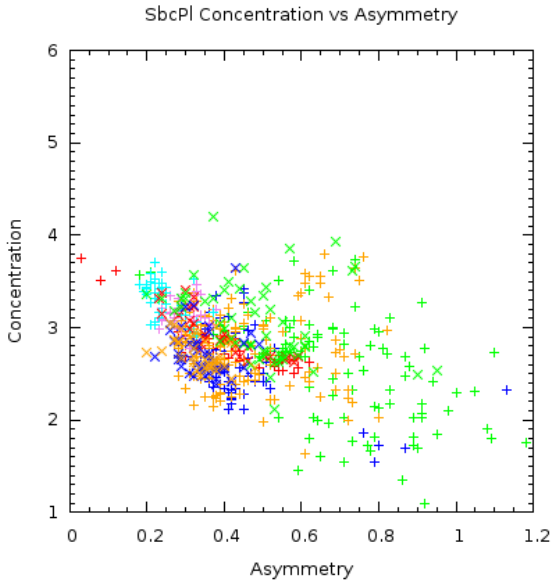

Figure 19. Plot of Concentration vs Asymmetry for the SbcPl simulation. The cyan remnant stage is confined to a relatively small region, but shares this region with data from nearly every other merger stage.

As before, plotting this same data against a third parameter, LIR/g in this case, gives us a spread of the data over the new axis that helps distinguish different merger stages. This is shown in Figure 20. Now, however, there is far more clutter in the cyan merger region of this plot than in the NUV-r vs Gini vs M20 plots, making it nearly impossible to define a region in this parameter space that is characteristic to only the remnant stage.

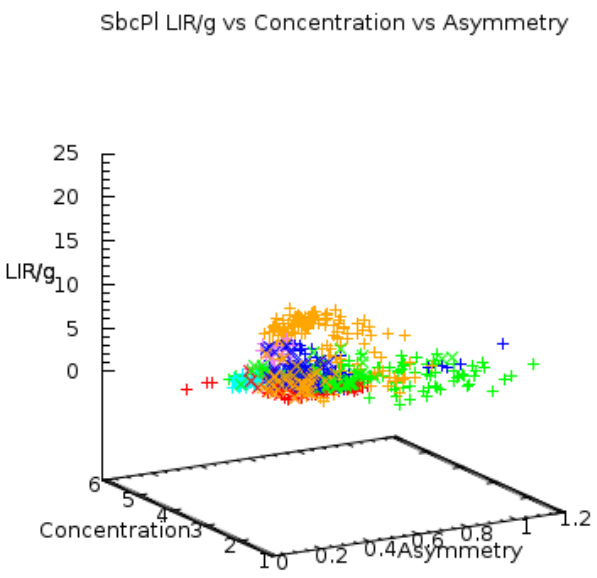

Figure 20. A plot of LIR/g vs Concentration vs Asymmetry for the SbcPl simulation. Note that the cyan remnant stage data in the lower-back-left region of the data plotted shares this region with data from many other merger stages.

The plot in Figure 21 has the exact same properties as the one preceding it, only this time the data with non-zero values of separation have been removed, leaving a very clear view of the isolated cyan remnant stage. This region of the following plot that holds the remnant stage is characteristic of nearly all the simulations, and plots similar to this one for those simulations may be found in the data section of the paper.

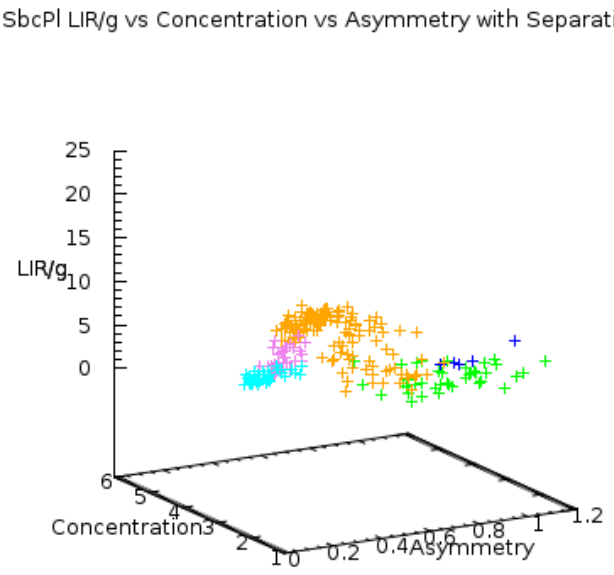

Figure 21. Plot of LIR/g vs Concentration vs Asymmetry for the SbcPl simulation, with non-zero values of separation removed. By subtracting the data that can be clearly seen as two distinct galaxies, the remaining data is much more easily isolated in their respective regions of the graph.

It was found rather generally, although unfortunately not completely generally, that the remnant stage in merging has a value greater than 4 for NUV-r and a value less than 4 for LIR/g. Regardless of precise value, these two colors have a strong correlation with the star formation rate of the galaxies. Characteristically, all of the mergers experience an increase in star formation rate during the maximal separation stage and a subsequent second increase in the final merger stage.

Figure 22 shows an observationally based color-magnitude diagram of data from the GALEX (GALaxy Evolution eXplorer) taken from Salim et al. (2007). This plot includes data from every kind of galaxy observed in the local universe, and is split up in the various frames of the figure according to the sort of activity of the galaxy. This data naturally includes mergers but most of the galaxies will be non-interacting because only a fraction of galaxies in the universe are interacting. The top center plot in the Figure 22 shows only galaxies for which there is prevalent star formation, while the bottom right plot of this figure shows galaxies without Hα absorption lines, indicating a lack of star formation.

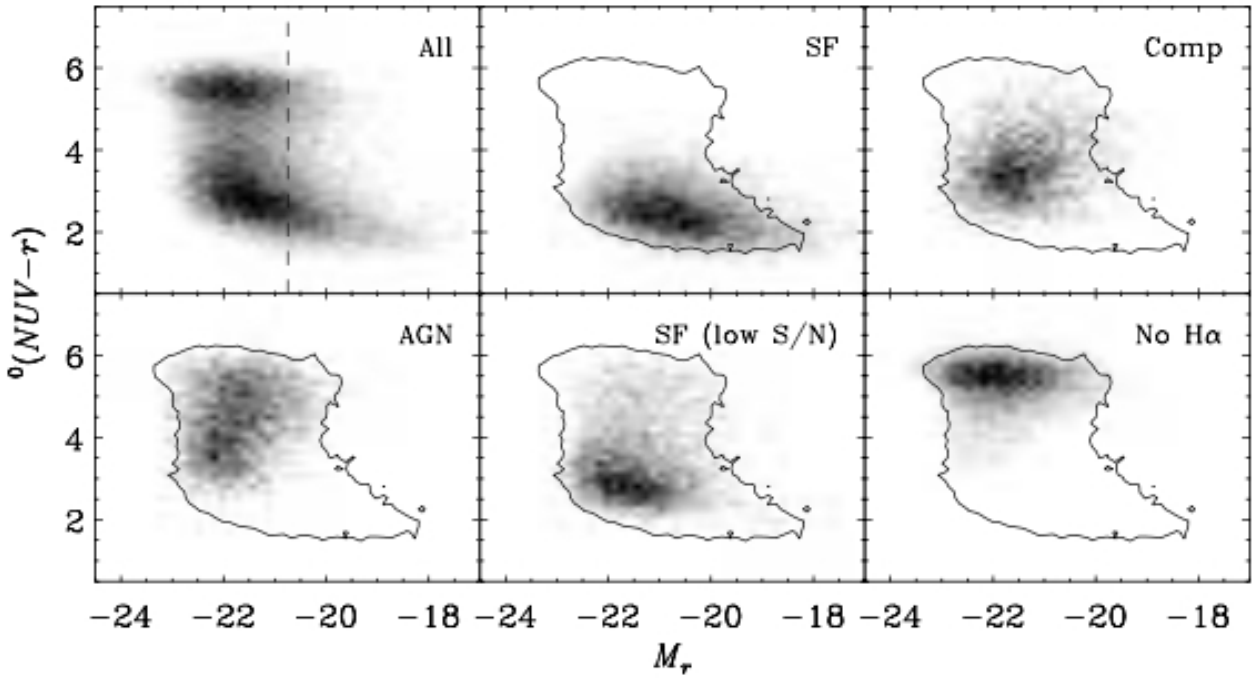

Figure 22. Color magnitude diagrams of galaxies observed in the local universe, from Salim et al. (2007). The darker the pixels, the more galaxies are in that region of the plot. The first image includes all galaxies observed in the GALEX survey and shows a distinct separation between galaxies with and without prevalent star formation. Subsequent plots show separated parts of this same data with star-forming galaxies alone in the top center, a composite of star-forming galaxies and AGN galaxies in the upper right, galaxies with active galactic nuclei at the bottom left, star-forming galaxies with low supernova activity in the lower center, and in the bottom right, galaxies with no Hα absorption lines, indicating a lack of star formation.

In contrast, the galaxies in the simulations examined for this paper are exclusively interacting, and even in the latest stages of merging, there is typically at least some star formation taking place. The following color-magnitude diagram (Figure 23) was created from the Sbc merger simulation data (with n=2 feedback). The same quantities are being plotted as the observational data above, but notice the differences between them. First of all, the simulation data are all bluer (NUV-r is smaller) than the non-star-forming galaxies in the Salim plot. This is to be expected because, as just mentioned there is at least some star-formation taking place throughout the merging process and NUV-r has been shown to decrease with greater star-formation rates. The next thing to notice is that none of the simulation data

have as high magnitudes (low luminosities) as the observational data, which goes all the way up to about -18 in the horizontal SDSS r magnitude axis. The reason for this is that the Sbc galaxies in these simulations are all relatively massive galaxies, whereas the observational data in the Salim plot include all galaxies, many of which are comparatively very small, and will therefore be less luminous in all frequency bands, including r. With these two differences in mind, when comparing observational data to the theoretical simulation data, one can see that they are pretty consistent with one another. The majority of the data from the simulations spans from just under -23 and up to nearly -21.5 magnitudes in the r band, and reside mostly within the range of 2 to just above 4 in NUV-r. This puts the simulation data in the lower left region of observed of the total observed data in Salim's plot, which is the brighter (hence more massive) portion of the star-forming section of the plot, as one would expect.

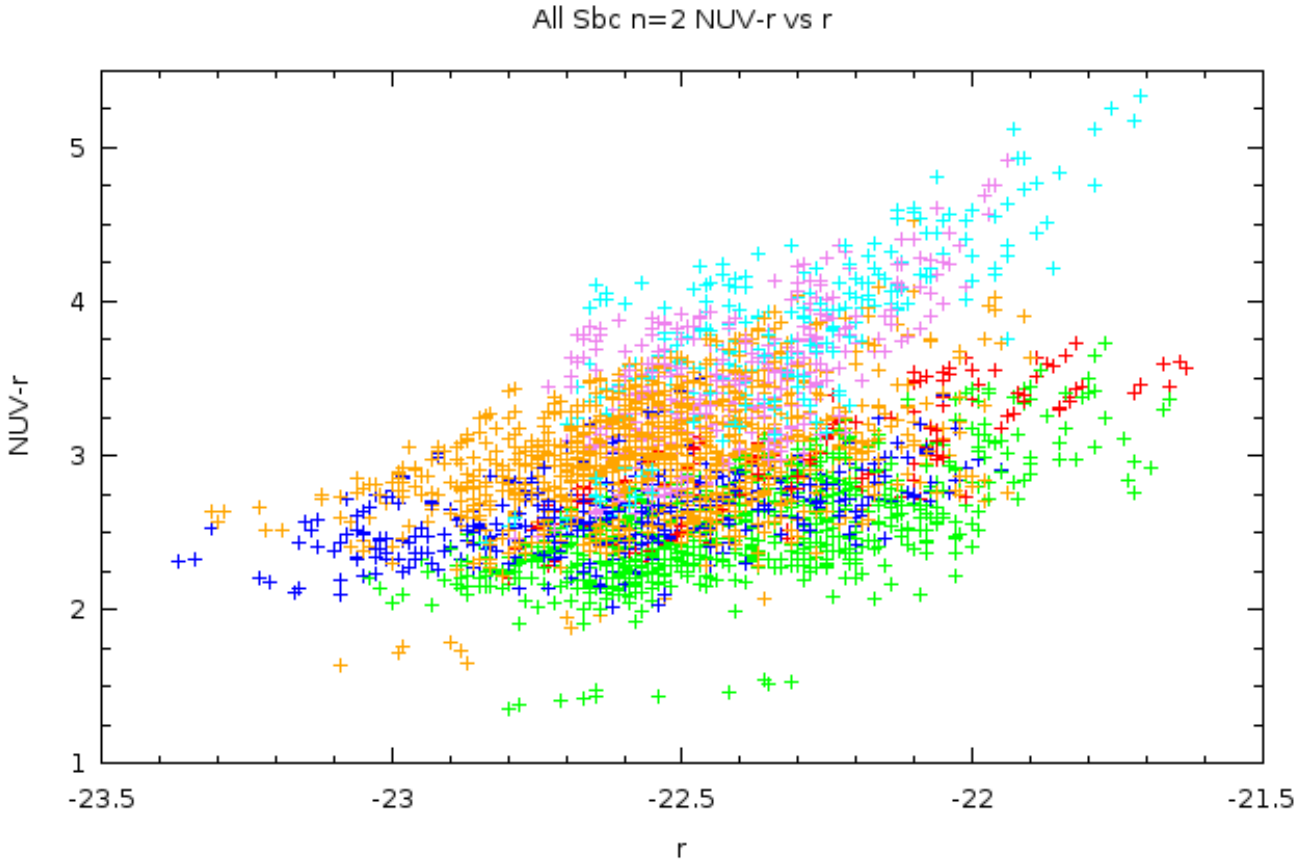

Figure 23. NUV-r vs r color magnitude diagram based on simulation data. This whole region of data corresponds to the brighter section of the the star-forming region of Samir Salim's plot above, indicating that the simulations are indeed consistent with observational data.

The Sbc galaxies plotted in the CMD are all relatively massive star-forming galaxies, which is why they only cover a small portion of the range of observational data shown Salim's observational CMD. Figure 24 shows a color-magnitude diagram for the G-G galaxy merger simulations, which span a large range in galactic mass (a factor of 23). Since there are only four G-G mergers examined, the difference in size between any of these mergers is also substantial, which is why they appear clearly distinct across the r magnitude axis. If there were even more simulations run with various masses lying between the masses of these G-G mergers, or also if one were to look at unequal mass mergers (such as a G2G1, for instance) one would expect that the space in between these data would be filled in. This plot, together with the Sbc merger CMD in Figure 23, now span a range in NUV-r (from as low as 1 and up to as high as 6, with a majority between 2 and 4) and a range in r (from just below -23 up to just above -18) that comprises the star-forming region of Salim's observational data in Figure 22 quite nicely. This confirms that the simulations examined in this paper are consistent with observation of the physical universe, as one would hope.

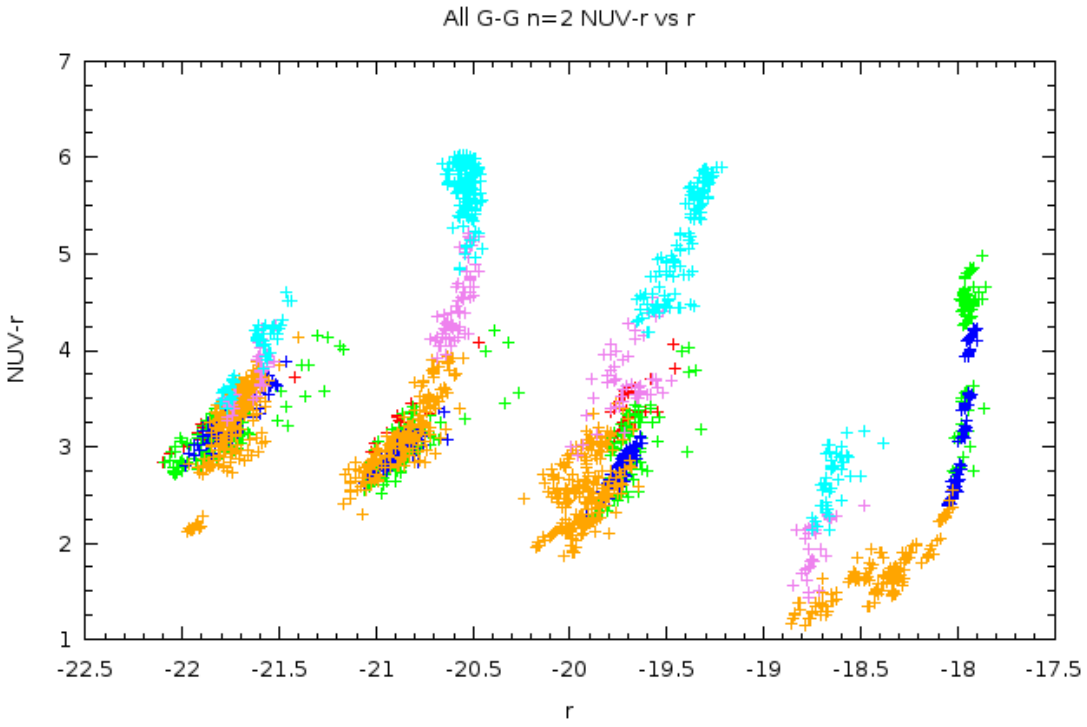

Figure 24. Color-magnitude diagram of G-G galaxy mergers. From left to right, the data show the G3G3, G2G2, G1G1, and G0G0 simulations as clearly distinct in such a plot. Together with the Sbc merger CMD above, these data inhabit the same region as the star-forming galaxies of Salim's observational plot.

Discussion

Described above are two ways to isolate the remnant stage from the other merger stages in the simulations. Although one may qualitatively see a trend in the properties of the remnant stage, relative to the other stages within a single simulation, and indeed across all simulations to an extent, there remains fluctuations in the vicinity of the remnant stage between each of the graphs as well as non-remnant points in the regions we would like to call remnant regions of the graphical space.

We did see, however, that going from a 2-dimensional morphology-morphology plot to a 3-dimensional morphology-morphology-color plot helps to further separate the merger stages into characteristic regions of their own. By examining a third variable along a third spatial dimension of the graph, data that may have been mixed with other merger stages in one region of the graph before will now be spread across this new dimension, making it possible to see distinct data points more clearly. If the examined stage has some characteristic value or range of values of this new parameter, looking at this 3-dimensional graph will not only spread out the data spatially, but will serve to confine the merger stage in question to a specific region within the 3-d space, as was demonstrated in the previous section with the addition of an NUV-r axis to the Gini vs M20 plots, and LIR/g axis to Concentration vs Asymmetry plots.

The remnant stage was given special attention because the distinction between remnant and merger a most critical distinction to make when using observational data as a basis for theoretical research. It is critical to know whether an elliptical-like galaxy, for instance, is indeed an elliptical galaxy, or if it is a late stage merger, if one is trying to use the data from that galaxy as a basis for a theory about the origin of elliptical galaxies, their black holes, and of active galactic nuclei activity in them. On the other hand, in order to study the whole merging process with more certainty regarding what stage a galaxy merger is undergoing, it would be useful to be able to characterize each one of the merger stages, instead of the remnant stage only. The same process described in this paper would be just as valid for characterizing any one of these stages, although different stages will have different characteristics, and hence will require a different set of parameters to be examined, in general. For further insight into what observable quantities may help to constrain other merger stages, you may refer to Seth Cotrell's 2004 undergraduate thesis, in which he creates an algorithm for the determination of merger stage of an older version of the SbcPP simulation.

Going from 2-d to 3-d plots can be very helpful in gaining insight into the characteristic properties of a merger stage, but this process may be extended even further, to higher dimensional spaces. It would not be possible to visualize graphs in 4, 5, 6, or more dimensions in a single graph, but a computer program could be made to examine all possible parameters for every simulation, and constrain each merger stage into a particular region of this N-dimensional hyperspace. With the addition of more variables considered at once, a given merger stage could be confined to a progressively more specific region within such a graph. The ideal result would be that a computer algorithm could examine every observable quantity from a given snapshot of a simulation, or observation, and be able to tell what stage the merger is undergoing and if it is indeed a merger at all, with some numerical measure of certainty, all without the need for human interpretation and the likely errors that could result from human interpretation.

In this paper, it has been shown how using seven different observable quantities, namely NUV-r, Gini, M20, LIR/g, Concentration, and Asymmetry, and Galaxy Separation can be used to help deduce whether or not a merger of any of the types described in this paper is in its remnant stage. This was done using two separate 3-d plots for each of the simulations considered. Considering these two plots together in one 6-dimensional space, together with the removal of non-zero separation values, would help isolate the remnant stage even more than one 3-dimensional plot would be capable of illustrating. Such a procedure is beyond the scope of this paper, however it is the writer's hope that his paper has illustrated the usefulness of such an approach.

Summary

Galaxies are typically classified as either spiral or elliptical, however a third group of galaxies called irregulars also exists, and these irregulars are often merging galaxies. Merging is a process that spans a few billion years and during this time, the stars in the galaxies do not typically collide or interact with one another. However, the stars' orbits around the galactic centers of the constituent galaxies are profoundly distorted by the presence of two massive black hole cores, with the net effect of destroying any disk or spiral arm structure of the colliding galaxies, leaving a single elliptical galaxy in their wake. Large clouds of dust within each of the galaxies do collide and interact, however, and the result of this collision is the formation of new stars. A large fraction of the light emitted by these young stars is blue light, emitted by the largest, brightest hottest-burning O and B stars, which only live a few million years before they explode, releasing even more energy. Since these stars have very short lifespans, compared to the lifespans of dimmer, redder stars as well as the duration of the merging process itself, the presence of the radiation produced by these bright blue stars gives a good indication of star formation. Such star-formation-indicating light includes ultra-violet light, because of the relatively high frequency of the blackbody peak of these stars. However, much of this light is absorbed by the same dust in which these stars were formed, which heats up and re-radiates this energy in the infra-red range of the electromagnetic spectrum.

Because one cannot observe a single galaxy merger from start to finish, due to the immense timescales involved in merging, simulations are needed to examine merging as a whole and dynamic process. An N-body hydrodynamic simulation program called GADGET was first run to simulate the the motion and behavior of the interacting galaxies, followed by a program called Sunrise which calculated the star formation, star age, and dust effects on outgoing light. A third program called Source Extractor used segmentation mapping to calculate the morphology of each galaxy and their product. The morphological quantities examined in this paper include Gini, M20, Concentration, Asymmetry, and Separation.

This morphology data, together with the color data output by Sunrise, is what was analyzed in this paper in order to find better methods for distinguishing between merger stages, especially the final remnant stage. The approach taken was to examine 3-dimensional plots of morphology vs. color intensity, chosen for the best possible isolation of the remnant stage from all other merger stage data in

the 3-d plots. It was found that NUV-r and LIR/g were two colors that had a tight correlation to star formation rate and hence galactic merger stage, and so these were the colors chosen for comparison to morphology data. In particular, NUV-r was plotted against Gini vs M20, and yielded a similar localization of remnant data within this plot for all of the simulations that were analyzed. Similarly, the remnant stage was also well isolated across all simulations using plots of LIR/g vs Concentration vs Asymmetry, with the data of non-zero values of separation removed, to help improve clarity.

The simulations dealt with in this paper cover a broad range of characteristics for the collisions of equal mass galaxies. This only scratches the surface of the possibilities of merging galaxies, which include unequal mass disk mergers, disk galaxies merging with elliptical galaxies of various sizes, as well as mergers of more than two galaxies at once. Already with equal mass merging, we see a wide variety of observable parameters and with increasing diversity in initial conditions, will come increasing differences in the results. Classifying such differing merger stages will require an extension of the techniques described in this paper, namely going to higher-dimensional plot spaces and using computer based statistical methods to determine the maximum isolation of each merger stage in such an N-dimensional plot, with a numerical result of what certainty data within each stage's region belongs to that stage. Such a process will require as many observables as are available including all morphology and every combination of colors possible. In addition, using such data eliminating techniques as the separation, used in this paper, will also be crucial in dividing up the data as well as possible. If a reliable algorithm can be created that enables a computer to automatically determine the merger state for an arbitrary type of galaxy merger, it would then be possible to distinguish mergers from non-mergers for a whole survey of galaxies all at once. By doing this one could then much more easily examine the correlation of AGN and other high energy phenomena to galactic merging to help test theory concerning the mechanism for super-massive black hole growth and as well as theory for other galactic phenomena that would not be approachable otherwise.

Data

Data

The following plots show color, morphology, and star-formation data for simulations examined in this paper. They were all constructed using GNUPlot. Each page contains data for a single merger, which is labeled above all the graphs. The sequential order of these pages goes as follows: SbcPP10x (SbcPP simulation run with ten times higher resolution.) , SbcPP , SbcPR , SbcRR , SbcPPr- , SbcPPr+ , SbcPl , SbcR , SbcPPn=0 (SbcPP simulation with n=0 feedback parameter. See Method section.) , SbcRn=0, (n=0 feedback) , G3G3 , G2G2

On each page the layout is the same and is as follows:

NUV-r vs Time	Gini vs M20
LIR/g vs Time	Concentration vs Asymmetry
SFR vs Time	NUV-r vs Gini vs M20
	LIR/g vs Concentration vs Asymmetry with Separation = 0

All of the plots that include time are aligned in one column so that NUV-r, LIR/g, and SFR may be compared to one another easily. The 3-dimensional plots are made so that the orientation of the plot for each type of merger is the same. By this it is meant that the NUV-r vs Gini vs Asymmetry plot for the SbcPP merger is rotated so that it has the viewing angle as the NUV-r vs Gini vs Asymmetry plot for every other merger, and the same goes for the LIR/g vs C vs A plots. This allows the reader to compare the different mergers as easily as possible. For both of these 3-d plots, a viewing angle was chosen to make most apparent the isolation of the cyan remnant stage from the other stages, across all of the simulations.

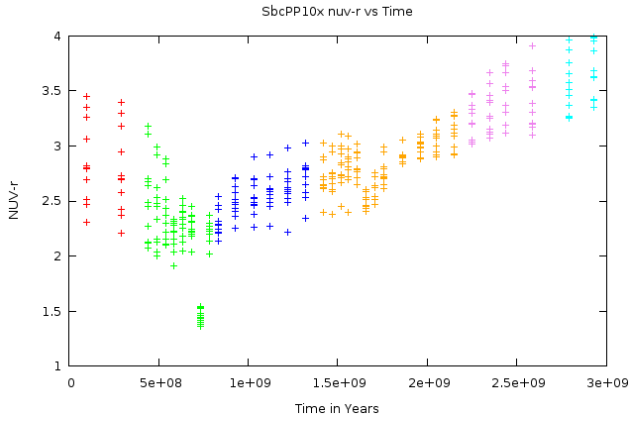
SbcPP10x nuv-r vs Time
NUV-r
Time in Years

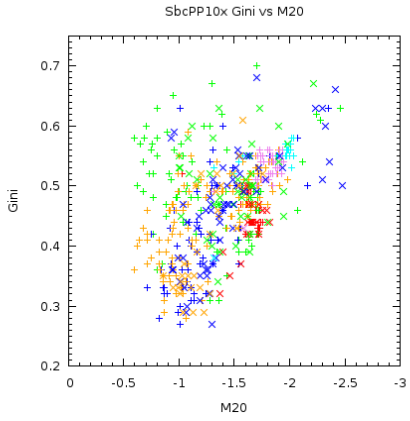
SbcPP10x Gini vs M20
Gini
M20

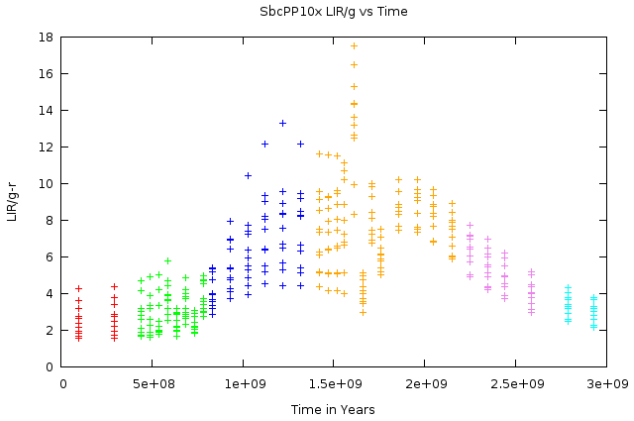
SbcPP10x LIR/g vs Time
LIR/g-r
Time in Years

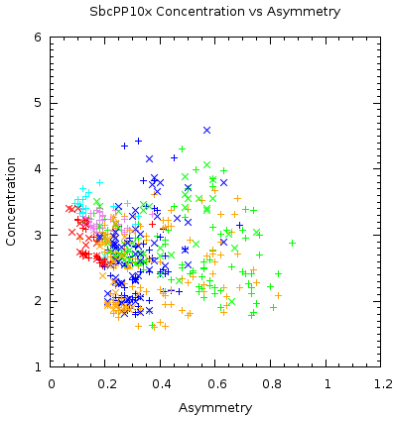
SbcPP10x Concentration vs Asymmetry
Concentration
Asymmetry

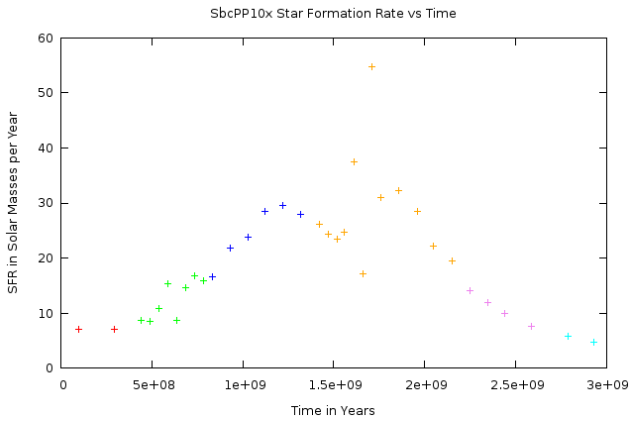
SbcPP10x Star Formation Rate vs Time
SFR in Solar Masses per Year
Time in Years

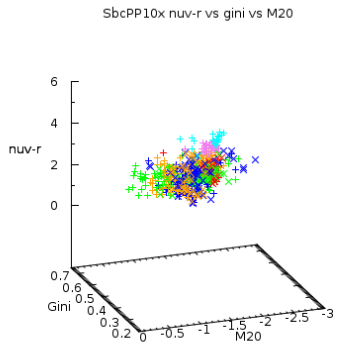
SbcPP10x nuv-r vs gini vs M20
nuv-r
Gini
M20

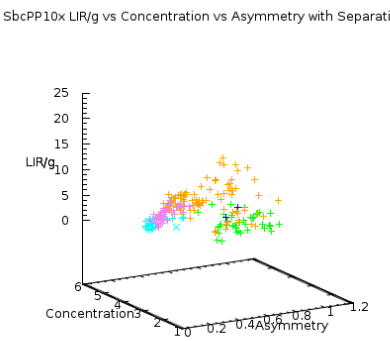
SbcPP10x LIR/g vs Concentration vs Asymmetry with Separation = 0
LIR/g
Concentration
Asymmetry

SbcPP10x

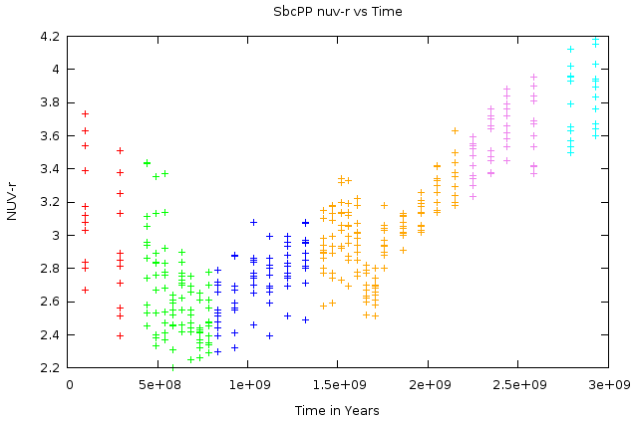
SbcPP nuv-r vs Time
NUV-r
Time in Years

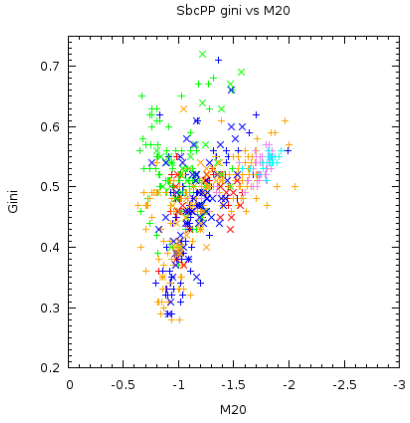
SbcPP gini vs M20
Gini
M20

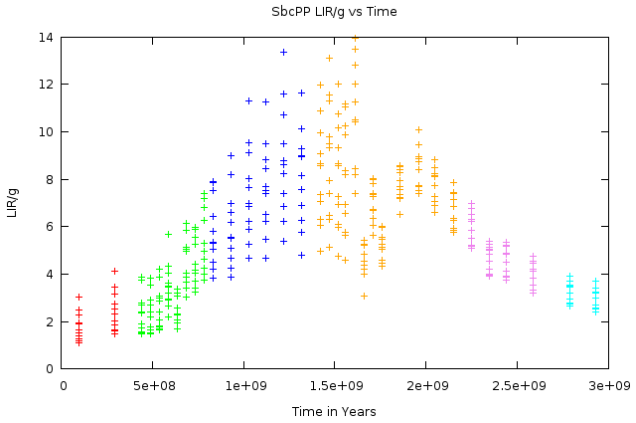
SbcPP LIR/g vs Time
LIR/g
Time in Years

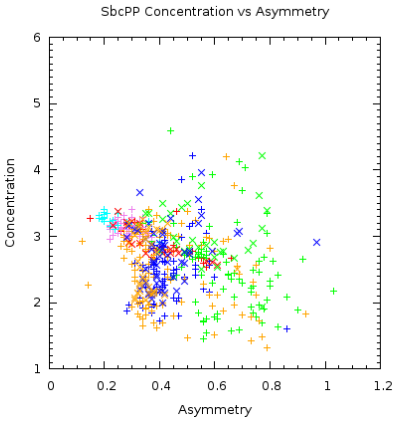
SbcPP Concentration vs Asymmetry
Concentration
Asymmetry

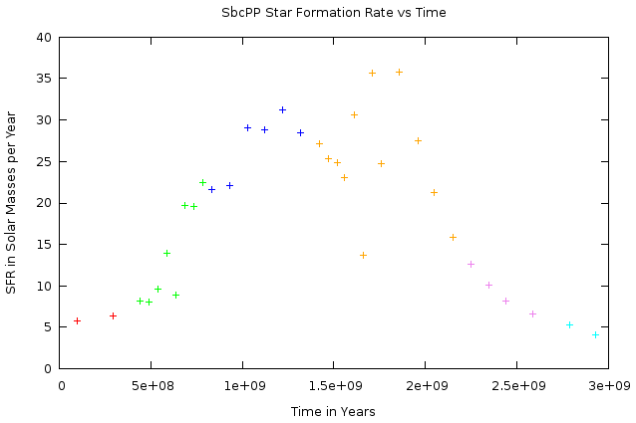
SbcPP Star Formation Rate vs Time
SFR in Solar Masses per Year
Time in Years

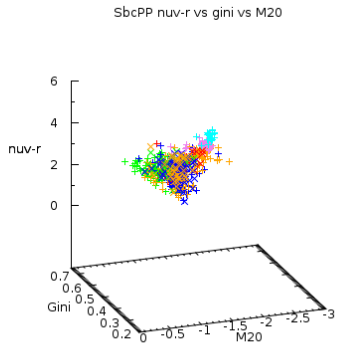
SbcPP nuv-r vs gini vs M20
nuv-r
Gini
M20

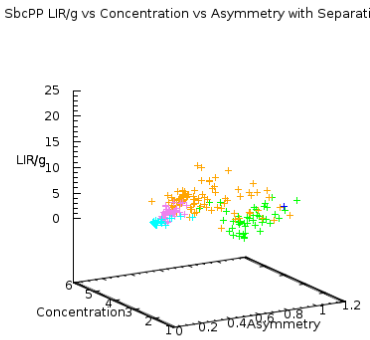
SbcPP LIR/g vs Concentration vs Asymmetry with Separation = 0
LIR/g
Concentration
Asymmetry

SbcPP

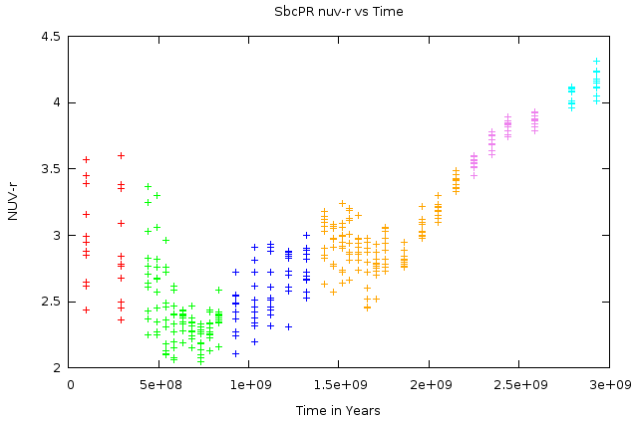
SbcPR nuv-r vs Time
NUV-r
Time in Years

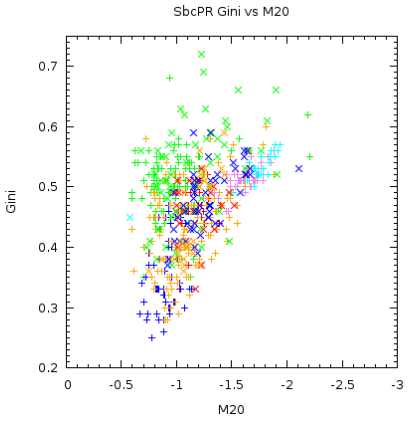
SbcPR Gini vs M20
Gini
M20

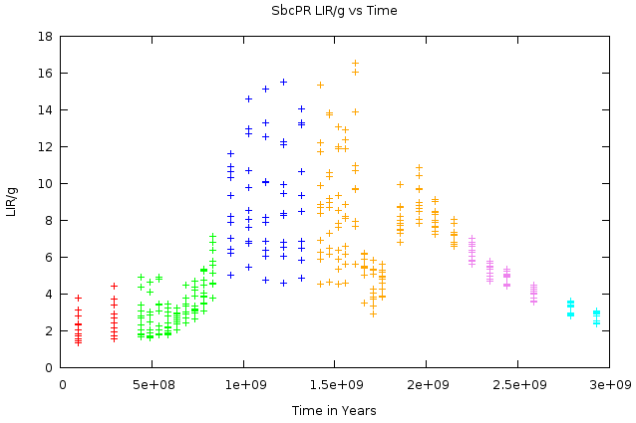
SbcPR LIR/g vs Time
LIR/g
Time in Years

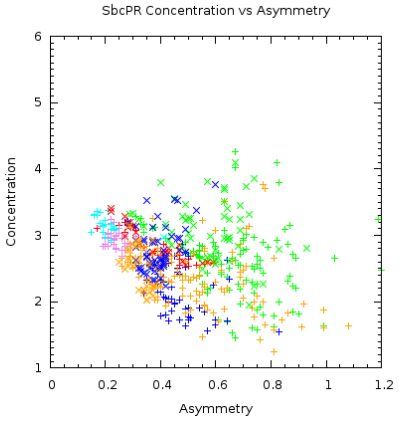
SbcPR Concentration vs Asymmetry
Concentration
Asymmetry

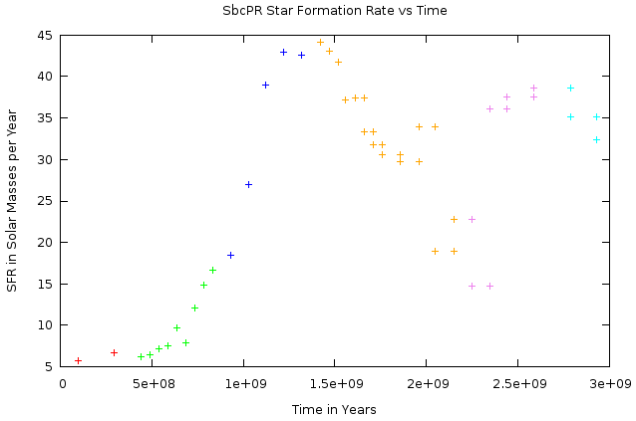
SbcPR Star Formation Rate vs Time
SFR in Solar Masses per Year
Time in Years

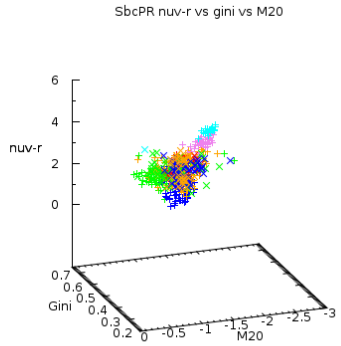
SbcPR nuv-r vs gini vs M20
nuv-r
Gini
M20

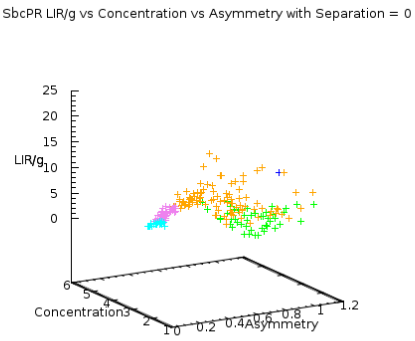
SbcPR LIR/g vs Concentration vs Asymmetry with Separation = 0
LIR/g
Concentration
Asymmetry

SbcPR

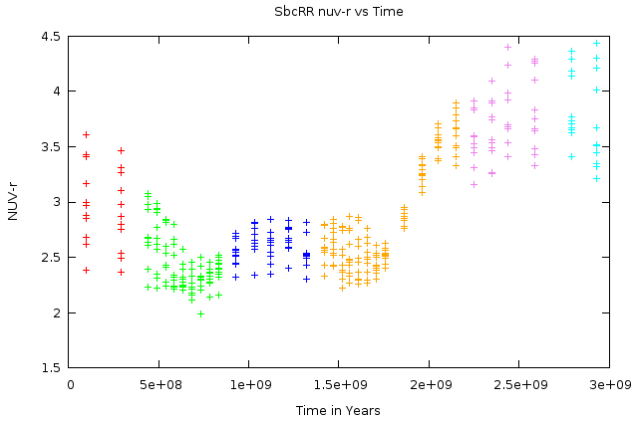
SbcRR nuv-r vs Time
NUV-r
Time in Years

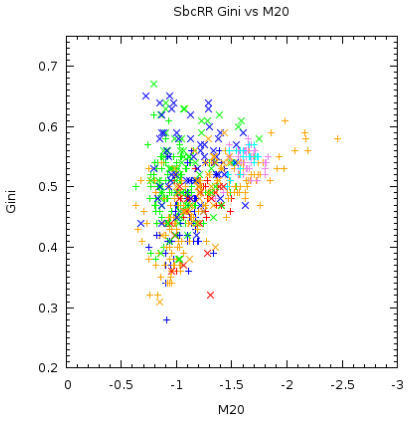
SbcRR Gini vs M20
Gini
M20

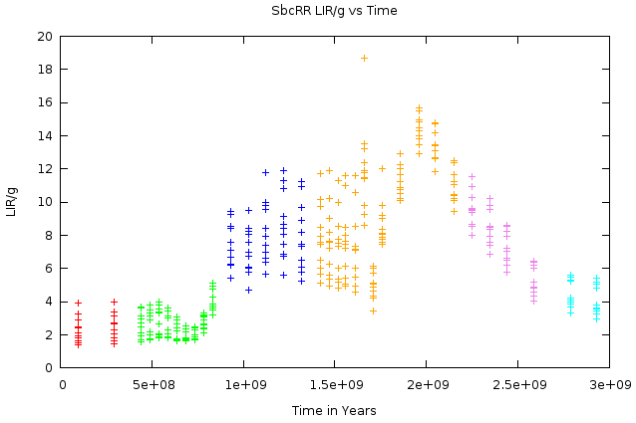
SbcRR LIR/g vs Time
LIR/g
Time in Years

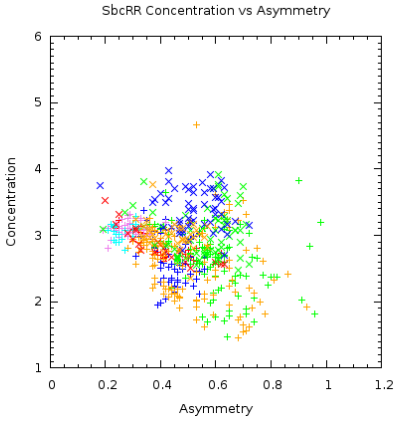
SbcRR Concentration vs Asymmetry
Concentration
Asymmetry

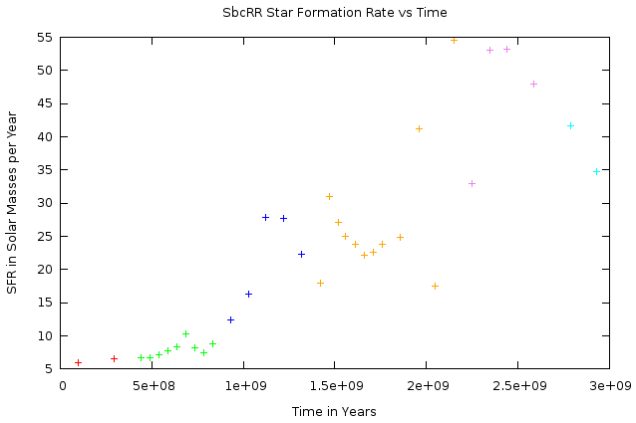
SbcRR Star Formation Rate vs Time
SFR in Solar Masses per Year
Time in Years

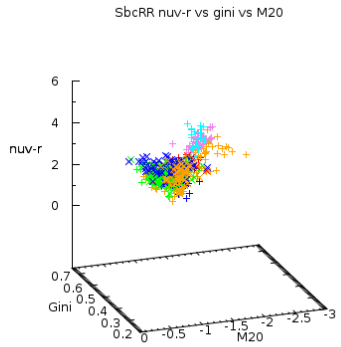
SbcRR nuv-r vs gini vs M20
nuv-r
Gini
M20

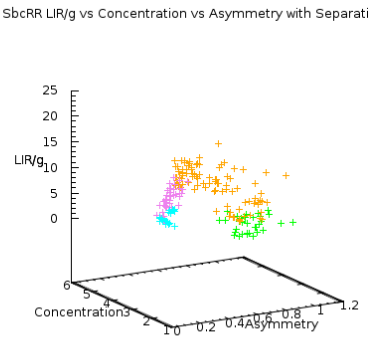
SbcRR LIR/g vs Concentration vs Asymmetry with Separation = 0
LIR/g
Concentration
Asymmetry

SbcRR

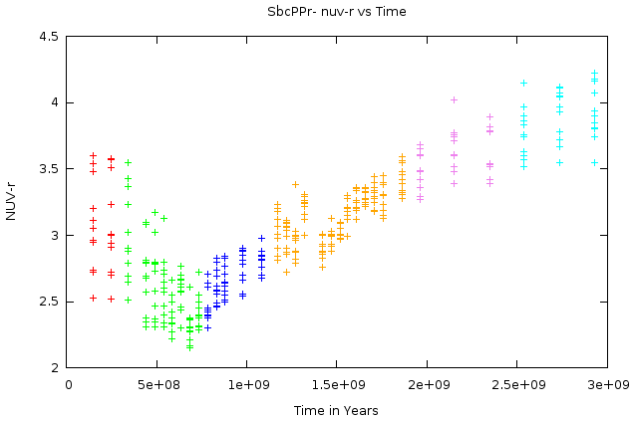
SbcPPr- nuv-r vs Time
NUV-r
Time in Years

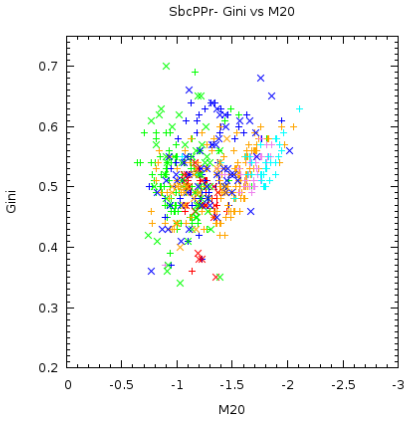
SbcPPr- Gini vs M20
Gini
M20

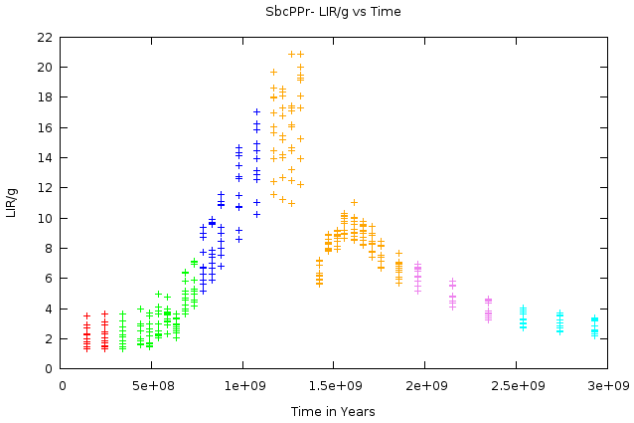
SbcPPr- LIR/g vs Time
LIR/g
Time in Years

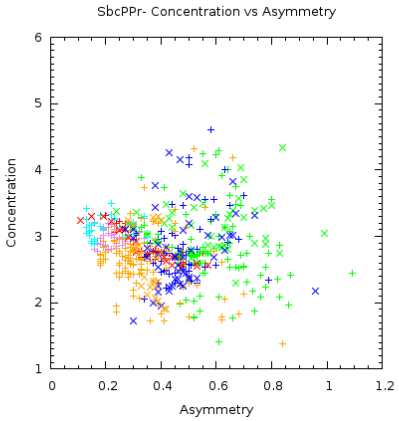
SbcPPr- Concentration vs Asymmetry
Concentration
Asymmetry

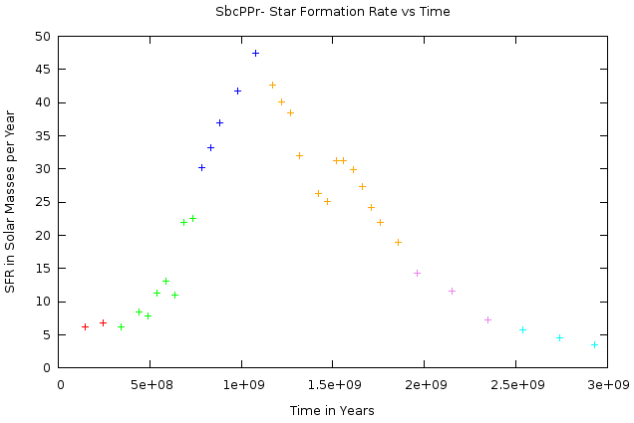
SbcPPr- Star Formation Rate vs Time
SFR in Solar Masses per Year
Time in Years

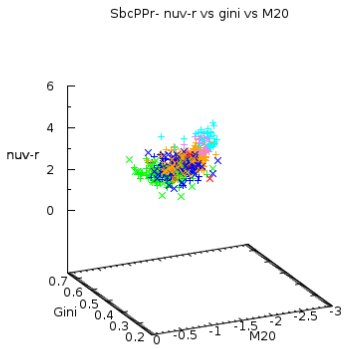
SbcPPr- nuv-r vs gini vs M20
nuv-r
Gini
M20

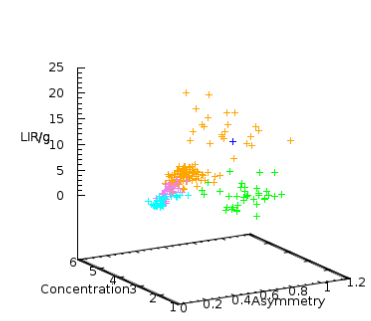
SbcPPr- LIR/g vs Concentration vs Asymmetry with Separation = 0
LIR/g
Concentration
Asymmetry

SbcPPr-

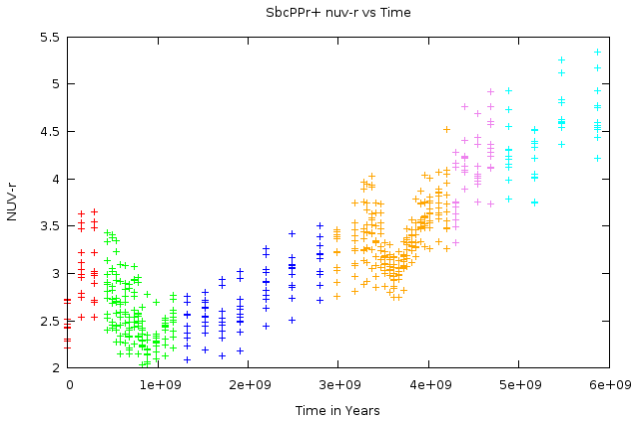
SbcPPr+ nuv-r vs Time
NUV-r
Time in Years

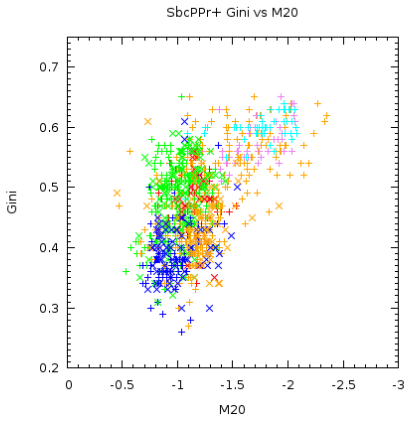
SbcPPr+ Gini vs M20
Gini
M20

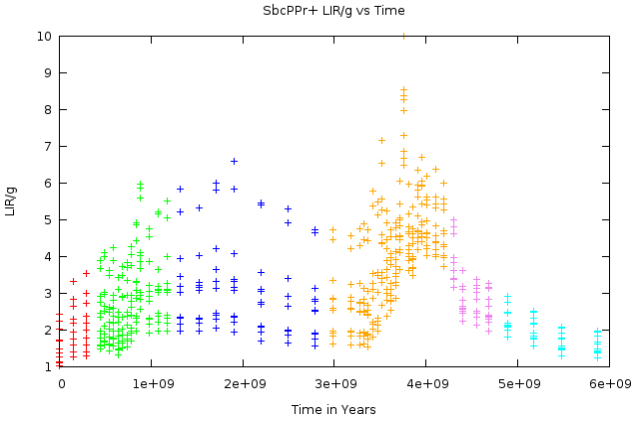
SbcPPr+ LIR/g vs Time
LIR/g
Time in Years

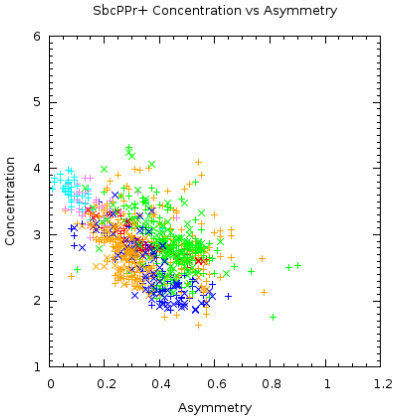
SbcPPr+ Concentration vs Asymmetry
Concentration
Asymmetry

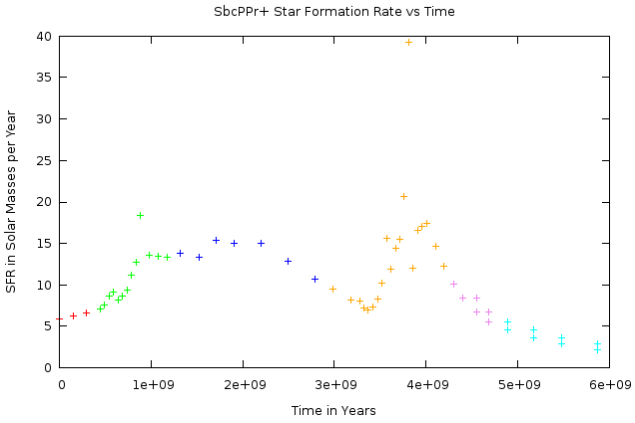
SbcPPr+ Star Formation Rate vs Time
SFR in Solar Masses per Year
Time in Years

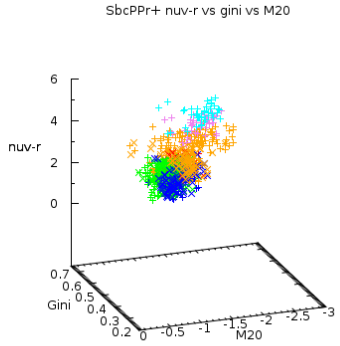
SbcPPr+ nuv-r vs gini vs M20
nuv-r
Gini
M20

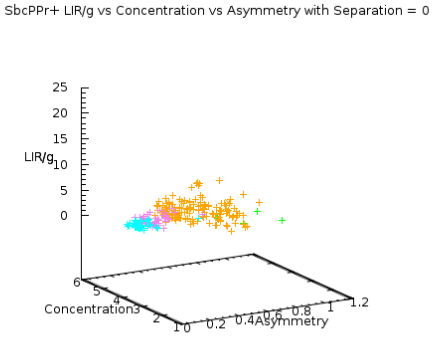
SbcPPr+ LIR/g vs Concentration vs Asymmetry with Separation = 0
LIR/g
Concentration
Asymmetry

SbcPPr+

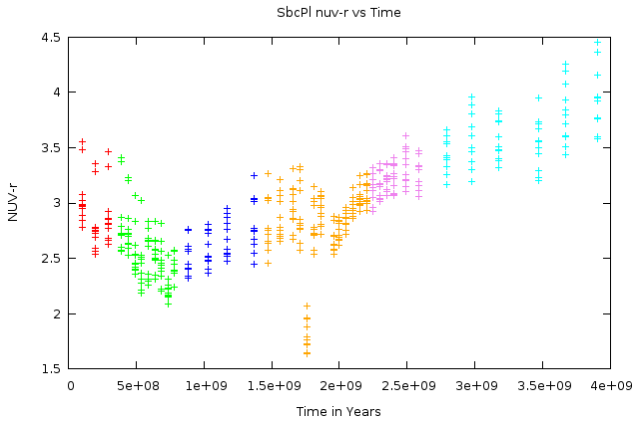
SbcPl nuv-r vs Time
NUV-r
Time in Years

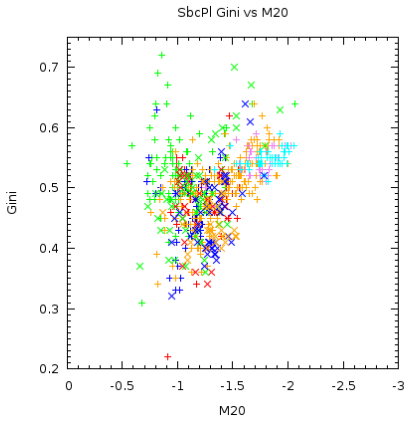
SbcPl Gini vs M20
Gini
M20

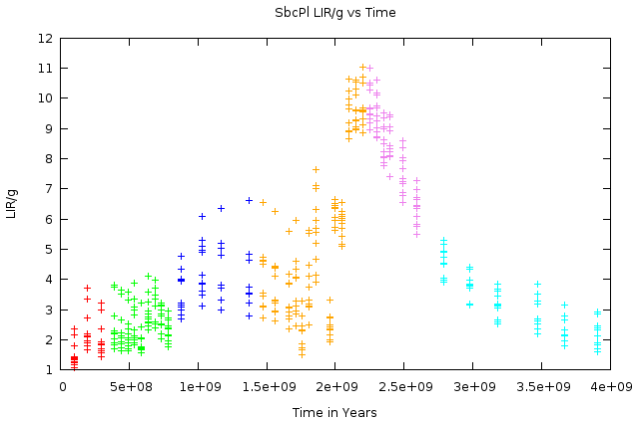
SbcPl LIR/g vs Time
LIR/g
Time in Years

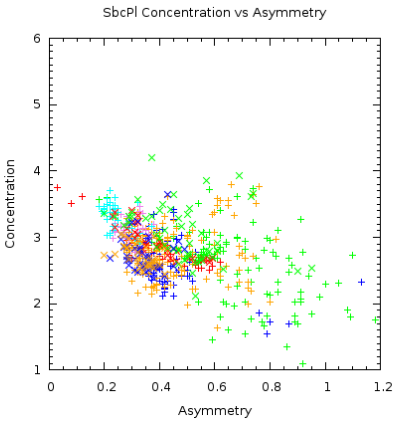
SbcPl Concentration vs Asymmetry
Concentration
Asymmetry

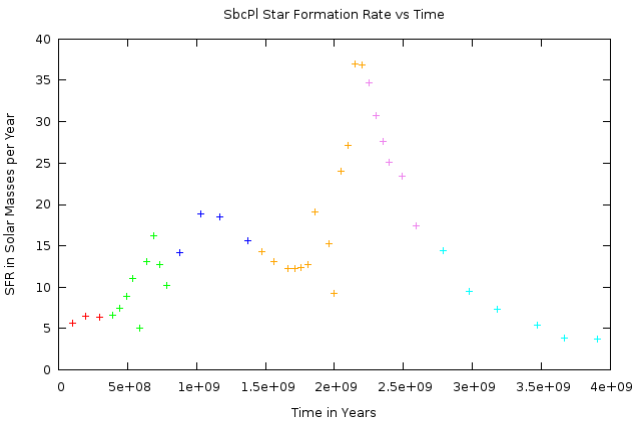
SbcPl Star Formation Rate vs Time
SFR in Solar Masses per Year
Time in Years

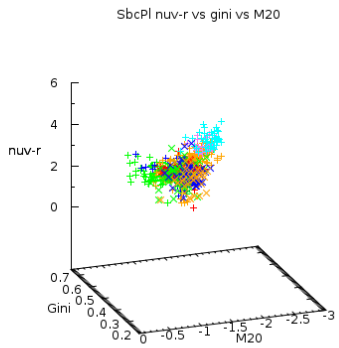
SbcPl nuv-r vs gini vs M20
nuv-r
Gini
M20

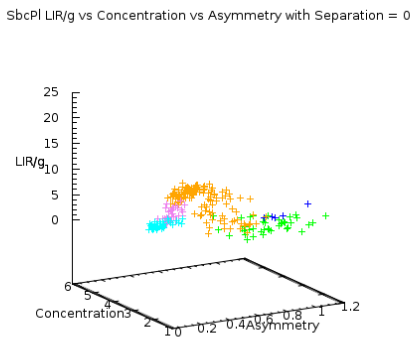
SbcPl LIR/g vs Concentration vs Asymmetry with Separation = 0
LIR/g
Concentration
Asymmetry

SbcPl

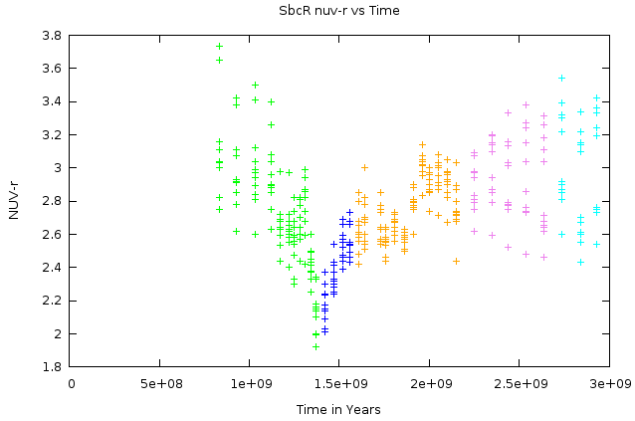
SbcR nuv-r vs Time
NUV-r
Time in Years

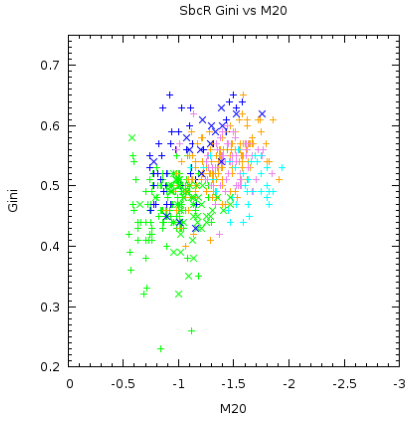
SbcR Gini vs M20
Gini
M20

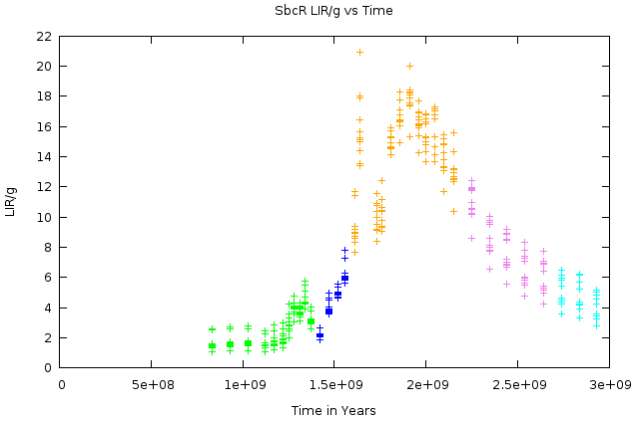
SbcR LIR/g vs Time
LIR/g
Time in Years

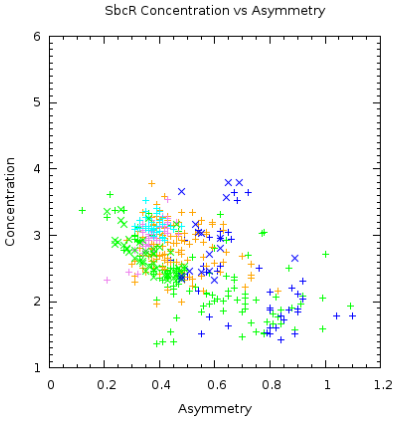
SbcR Concentration vs Asymmetry
Concentration
Asymmetry

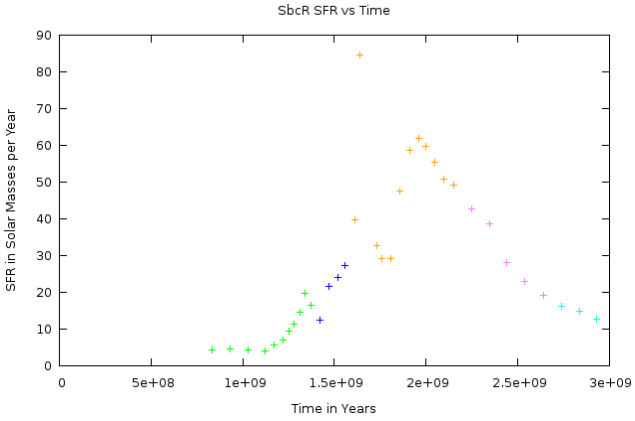
SbcR SFR vs Time
SFR in Solar Masses per Year
Time in Years

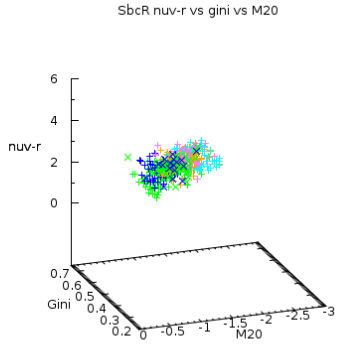
SbcR nuv-r vs gini vs M20
nuv-r
Gini
M20

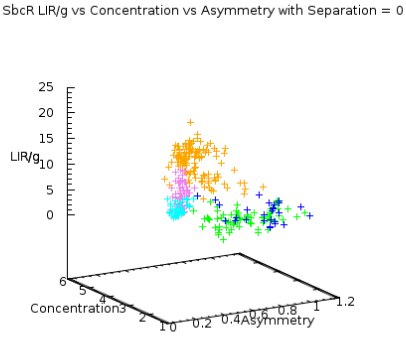
SbcR LIR/g vs Concentration vs Asymmetry with Separation = 0
LIR/g
Concentration
Asymmetry

SbcR

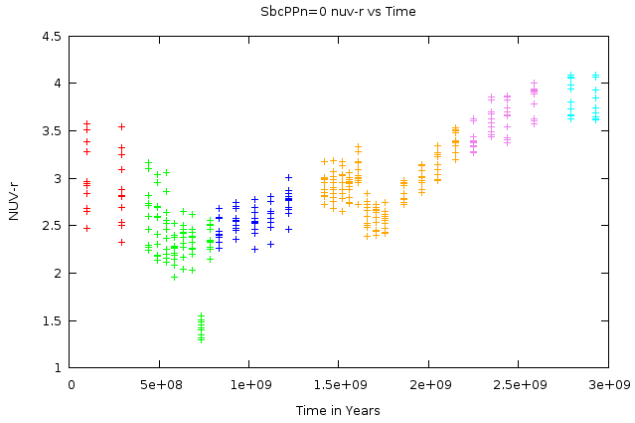
SbcPPn=0 nuv-r vs Time
NUV-r
Time in Years

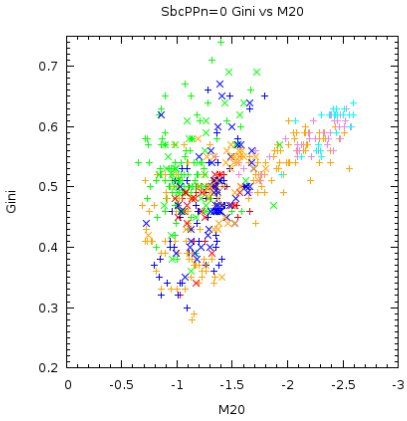
SbcPPn=0 Gini vs M20
Gini
M20

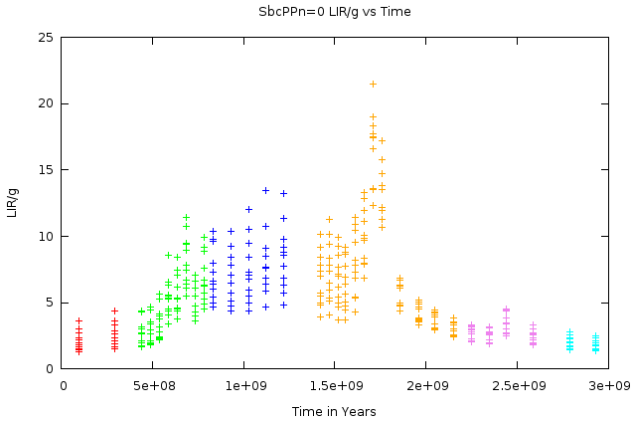
SbcPPn=0 LIR/g vs Time
LIR/g
Time in Years

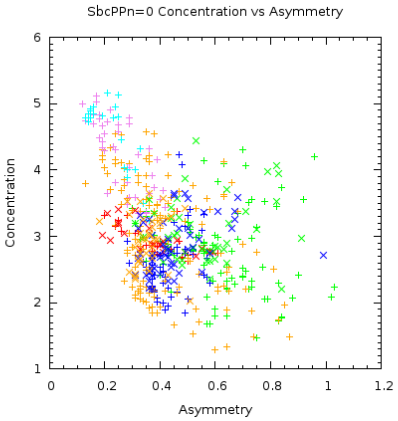
SbcPPn=0 Concentration vs Asymmetry
Concentration
Asymmetry

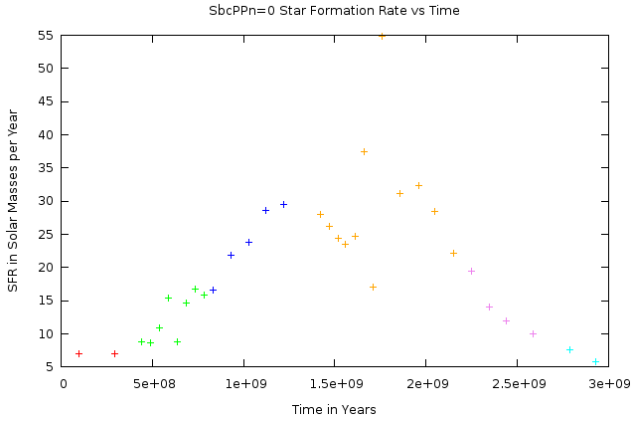
SbcPPn=0 Star Formation Rate vs Time
SFR in Solar Masses per Year
Time in Years

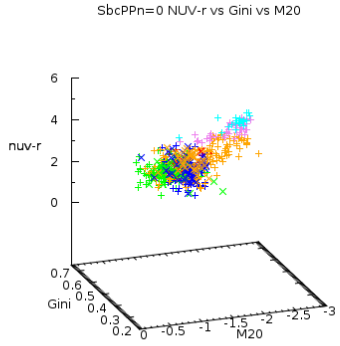
SbcPPn=0 NUV-r vs Gini vs M20
nuv-r
Gini
M20

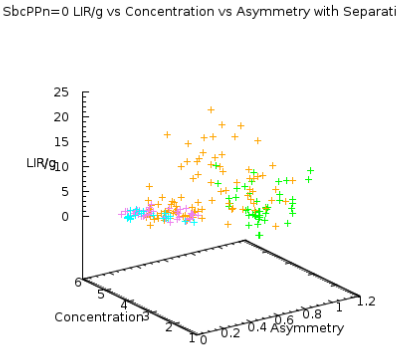
SbcPPn=0 LIR/g vs Concentration vs Asymmetry with Separation = 0
LIR/g
Concentration
Asymmetry

SbcPPn=0

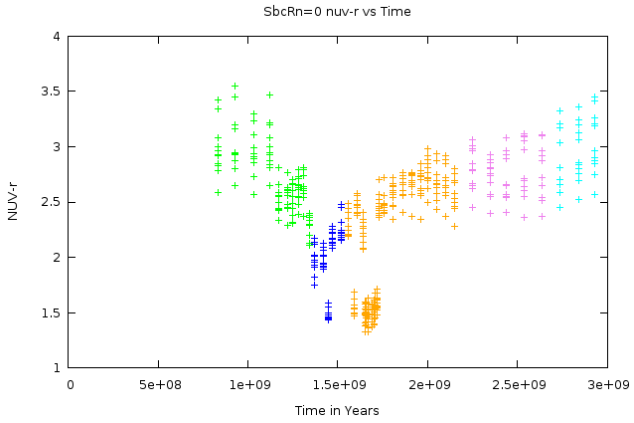
SbcRn=0 nuv-r vs Time
NUV-r
Time in Years

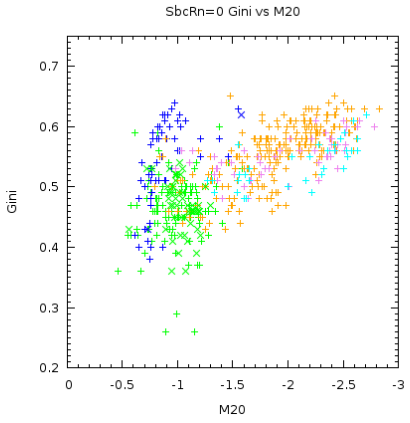
SbcRn=0 Gini vs M20
Gini
M20

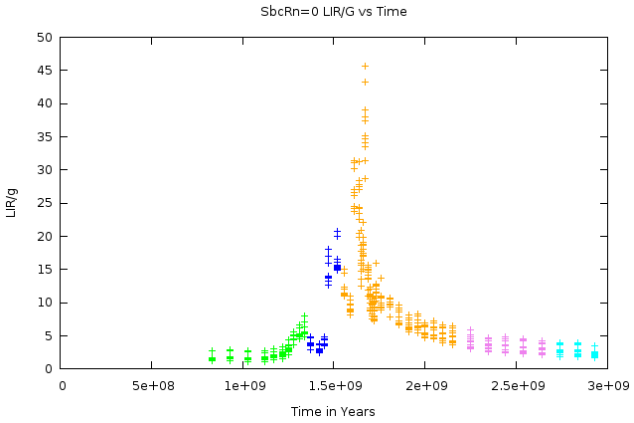
SbcRn=0 LIR/G vs Time
LIR/g
Time in Years

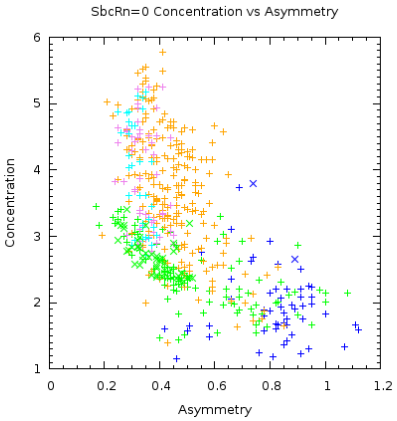
SbcRn=0 Concentration vs Asymmetry
Concentration
Asymmetry

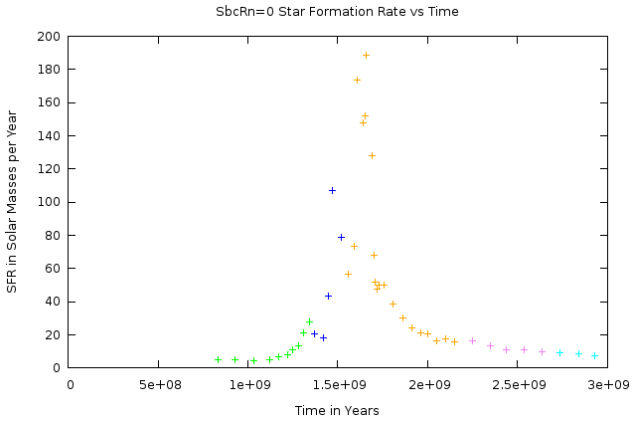
SbcRn=0 Star Formation Rate vs Time
SFR in Solar Masses per Year
Time in Years

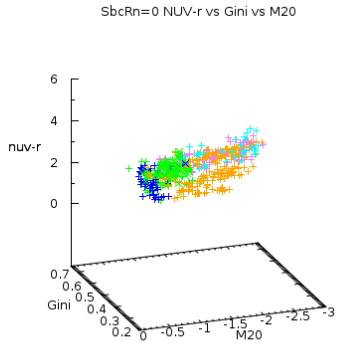
SbcRn=0 NUV-r vs Gini vs M20
nuv-r
Gini
M20

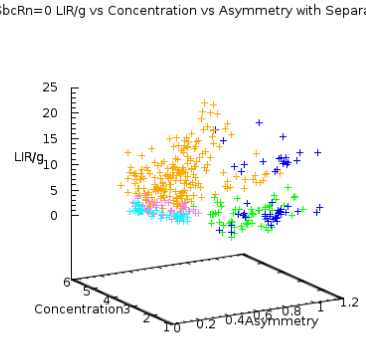
SbcRn=0 LIR/g vs Concentration vs Asymmetry with Separation = 0
LIR/g
Concentration
Asymmetry

SbcRn=0

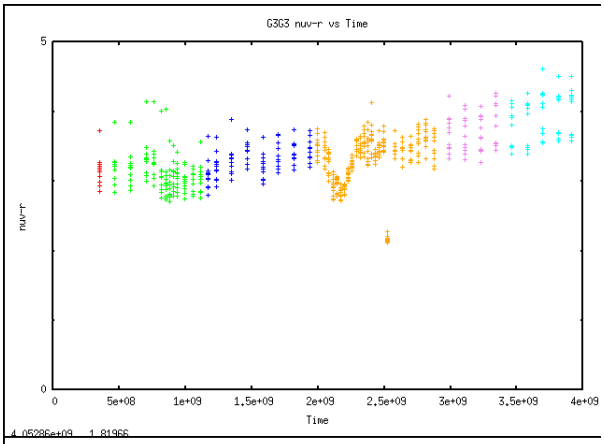
G3G3 nuv-r vs Time
nuv-r
Time
0
5e+08
1e+09
1.5e+09
2e+09
2.5e+09
3e+09
3.5e+09
4e+09
0
5

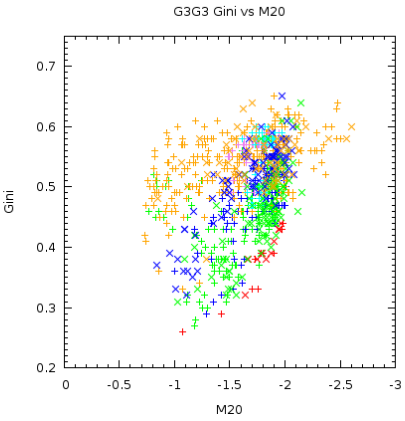
G3G3 Gini vs M20
Gini
M20
0.2
0.3
0.4
0.5
0.6
0.7
0
-0.5
-1
-1.5
-2
-2.5
-3

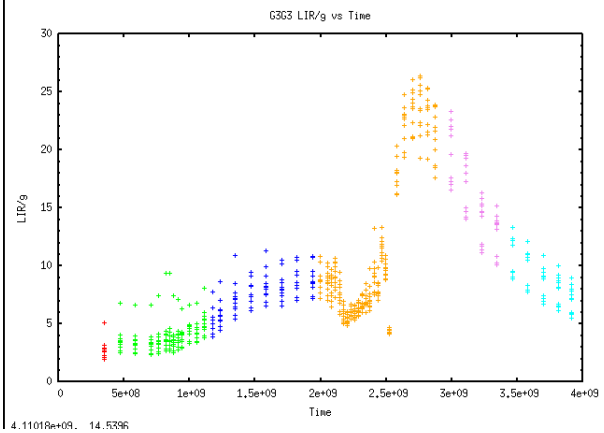
G3G3 LIR/g vs Time
LIR/g
Time
0
5e+08
1e+09
1.5e+09
2e+09
2.5e+09
3e+09
3.5e+09
4e+09
0
5
10
15
20
25
30

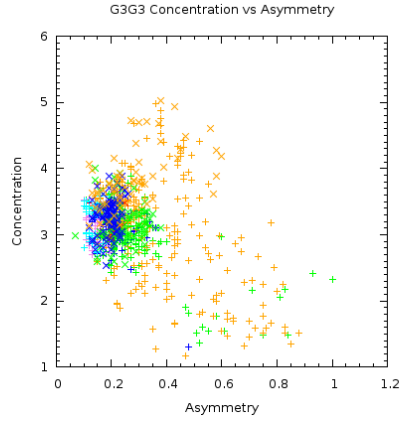
G3G3 Concentration vs Asymmetry
Concentration
Asymmetry
1
2
3
4
5
6
0
0.2
0.4
0.6
0.8
1
1.2

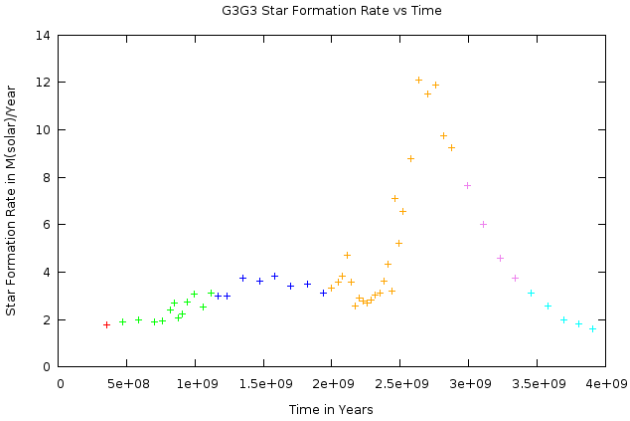
G3G3 Star Formation Rate vs Time
Star Formation Rate in M(solar)/Year
Time in Years
0
2
4
6
8
10
12
14
0
5e+08
1e+09
1.5e+09
2e+09
2.5e+09
3e+09
3.5e+09
4e+09

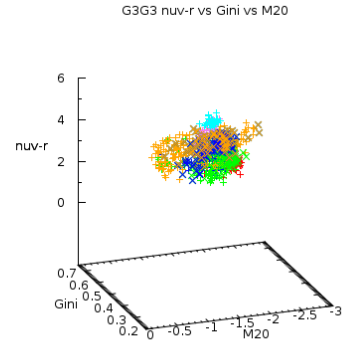
G3G3 nuv-r vs Gini vs M20
nuv-r
Gini
M20
0
2
4
6
0.2
0.3
0.4
0.5
0.6
0.7
0
-0.5
-1
-1.5
-2
-2.5
-3

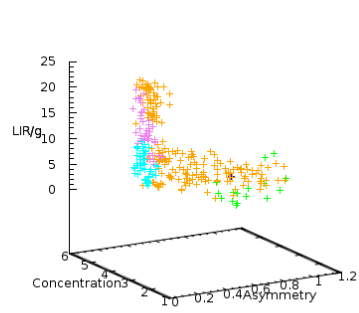
G3G3 LIR/g vs Concentration vs Asymmetry with Separation = 0
LIR/g
Concentration3
Asymmetry
0
5
10
15
20
25
1
2
3
4
5
6
0.2
0.4
0.6
0.8
1
1.2

G3G3

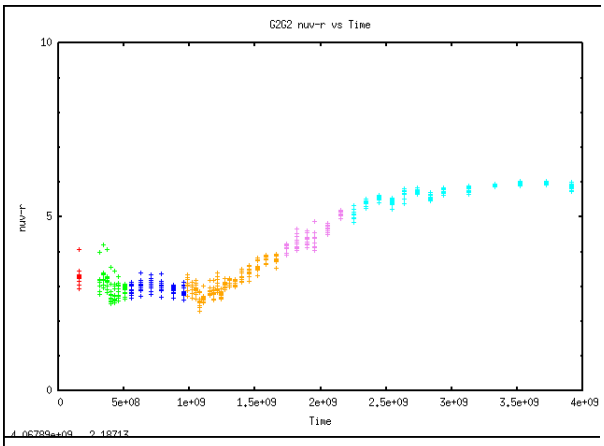
G2G2 nuv-r vs Time
nuv-r
Time

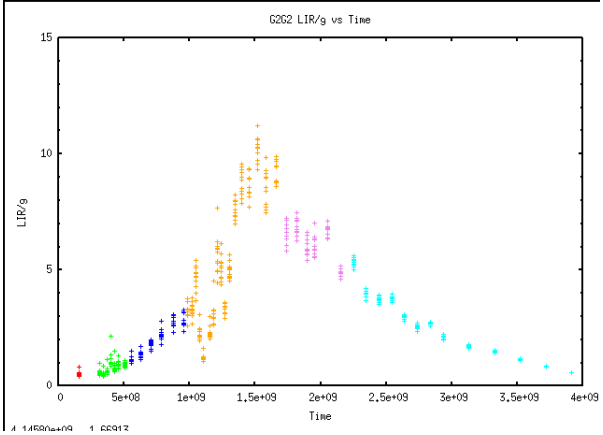
G2G2 LIR/g vs Time
LIR/g
Time

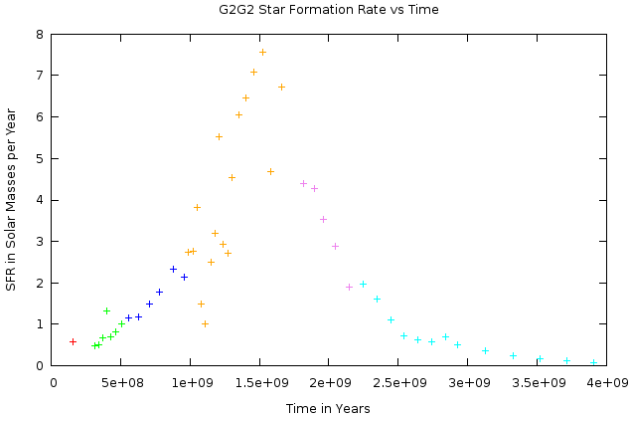
G2G2 Star Formation Rate vs Time
SFR in Solar Masses per Year
Time in Years

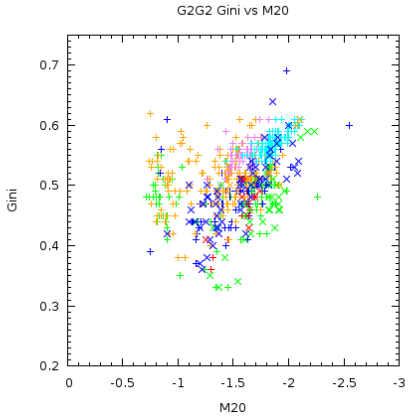
G2G2 Gini vs M20
Gini
M20

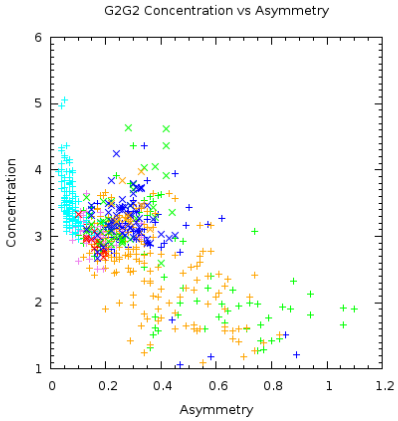
G2G2 Concentration vs Asymmetry
Concentration
Asymmetry

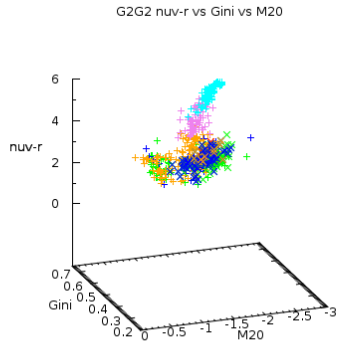
G2G2 nuv-r vs Gini vs M20
nuv-r
Gini
M20

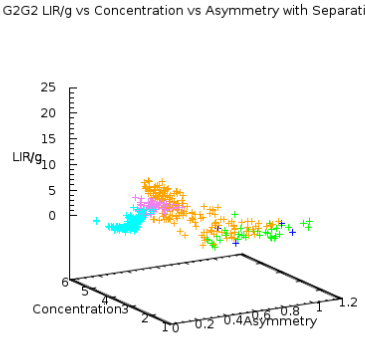
G2G2 LIR/g vs Concentration vs Asymmetry with Separation = 0
LIR/g
Concentration
Asymmetry

G2G2

References

Abraham, R., van den Bergh, S., & Nair, P. 2003, ApJ, 588, 218

Ciotti, L., Ostriker, J.P. 2007, arXiv:astro-ph/0703057v2

Cotrell, S. 2004, Undergraduate thesis, UC Santa Cruz

Cox, T.J., Primack, J.R., Jonsson, P., & Somerville, R.S. 2004, ApJL, 607, L87

Cox, T.J., Jonsson, P., Primack, J.R., Somerville, R.S. 2006, MNRAS, 373, 1013

Glasser, G.J. 1962, Amer. Stat. Assoc. 57, 648, 654

Hopkins, P.F., Hernquist, L., Cox, T.J., Keres, D. 2007, arXiv:0706.1243v2 [astro-ph]

Jonsson, Patrik 2004, Ph.D. thesis, UC Santa Cruz

Lotz, J.M., Primack, J., & Madau, P. 2004, AJ, 613, 262 (LPM04)

Lotz, J.M., Jonsson, P., Cox, T.J., Primack, J.R.